Chapter 9

Marine Gravity and Geoid from Satellite Altimetry

O.B. Andersen,

Geodetic Department,
DTU-Space,
Juliane Maries Vej 30,
DK-2100, Denmark

Email: oa@space.dtu.dk

Table of Contents

9.0 Outline of the chapter....3
9.1 Altimetry data....3
9.2 Retracking....6
9.3 Sea surface height observations....7
9.3.1 Mean sea surface and mean dynamic topography....10
9.3.2 Remove-restore for satellite altimetry....11
9.3.3 Dynamic sea surface topography....12
9.4 Crossover adjustment....14
9.5 Data editing, data quality and error-budget....17
9.6 Gravity recovery from altimetry....20
9.7 Least Squares Collocation for altimetry....21
9.7.1 Interpolation using least Squares Collocation....24
9.8 Deterministic methods....25
9.9 Fast spectral methods for altimetric gravity prediction....26
9.9.1 Fast Fourier Techniques for altimetric gravity....27
9.9.2 Filtering....29
9.10 Practical computation of global high resolution marine gravity....30
9.10.1 North Sea example....34
9.11 Accuracy of present-day altimetric marine gravity fields....37
9.12 Integrating marine, airborne and satellite derived gravity....39
9.12.1 East Greenland airborne and altimetric gravity example....40
9.13 Altimetric gravity research frontiers....41
9.13.1 ICESat and Cryosat-2....41
9.13.2 Altimeter range corrections....43
9.13.3 Ocean tides....44
9.13.4 Retracking in coastal and Polar Regions....45
Appendix 9.1. Data resources....48

Abbreviations

AVISO Archivage, Validation et Interprétation des données des Satellites
CHAMP CHAllenging Minisatellite Payload (German satellite)
CRYOSAT Cryosphere Satellite
DNSC Danish National Space Centre
DOV Deflection of the vertical
ECMWF European Centre for Medium-range Weather Forecasts
EIGEN European Improved Gravity model of the Earth
EGM Earth Gravity Model
ERM Exact Repeat Mission
ERS European Remote-sensing Satellite
ESA European Space Agency
Envisat Environmental Satellite
EUMETSAT Eur. Organ. for the Exploitation of Meteorological Satellites
FFT Fast Fourier Technique
GM Geodetic Mission
GGM Global Geopotential Model
ICESat Ice, Cloud and Elevation Satellite
JPL Jet Propulsion Laboratory
Geosat Geodetic Satellite
GFO Geosat Follow-On
GOCE Goddard Ocean Tide model
GPS Global positioning system
GRACE Gravity Recovery and Climate Experiment
GRAVSOFT Gravity prediction Software
GSFC Goddard Space Flight Center
KMS Kort- og Matrikelstyrelsen (National Survey and Cadastre, Denmark)
LSC Least Squares Collocation
MDT Mean Dynamic Topography
MSS Mean Sea Surface
NCTU National Chaotung University (Taiwan)
NOAA National Oceanic and Atmospheric Administration
OSU Ohio State University
PO.DAAC Physical Oceangraphy Distributed Active Archiving Center
RADS Radar Altimeter Database System (http://rads.tudelft.nl/)
RMS Root Mean Square
SAR Synthetic Apertur Radar
SRAL/SIRAL Syntetic Interferometric Radar Altimeter
SS Sandwell and Smith
SWH Significant Wave Height
TOPEX Topography Experiment

9.0 Outline of the chapter

Two thirds of the globe is covered with water, and large parts of the ocean are not covered with marine gravity observations. In large parts of the Southern Pacific Ocean the distance between surveys lines are several hundred kilometres thus only resolving signals of twice that distance. Satellite altimetry can provide information of the height of the oceans over nearly 60% of the Earth surface. These data can be used to derive a high resolution global marine gravity field with an accuracy ranging between 2 - 4 mGal.
In this chapter satellite altimetric data are introduced and the importance to global geoid and gravity mapping are demonstrated. Individual satellite altimetry observations might not provide as accurate measure of the gravity field as those by marine gravity, but the ability to provide a near global uniform accurate gravity field makes satellite altimetry un-surpassed and essential for determining the high resolution global marine gravity field of the Earth.

Initially the altimetric sea surface height observations is described. Then the process of isolating residual geoid signal is covered. Subsequently, methods for converting altimetric sea surface height observations and/or sea surface slopes to global marine gravity are described. The accuracy of the global marine gravity field is presented along with methods for combining satellite altimetry with marine and airborne gravity using least squares collocation. Finally some of the current frontiers and trends in development of next generation global marine gravity fields are covered.

9.1 Altimetry data

Prior to the space age global marine geoid and gravity field mapping of the worlds ocean relied on sparse measurements from surveying ships and tide gauge stations located along irregular local coastline. During the last three decades, satellite radar altimetry has revolutionized marine geodesy and proven to be an essential tool for recovery of the global marine geoid and gravity field especially in areas of sparse ship coverage (Zlotniki, 1984). Individual satellite altimetry observations might not provide as accurate direct gravity field observations as marine gravity, but the ability to provide near global accurately gravity field makes satellite altimetry un-surpassed for determining the global marine gravity field of the Earth.

Altimeter observations of sea surface height offer a fundamentally different way to measure the local gravity than that provided by space gravity missions such as GRACE, CHAMP or GOCE. Space gravity missions measure the gravity field directly at an altitude of 250-700 km. However, due to upward continuation short wavelength scale features in the gravity field is attenuated. Consequently only long wavelength features can be obtained from space gravity field missions. In terms of space-borne instrumentation only altimeters can measure the high resolution gravity field from space (in the range of 5-100 km). This is because the satellite altimetry indirectly measures gravity via measuring the geoid height variations at the sea-surface (by measuring sea surface height variations). Hereby satellite altimetry provide observations directly at the sea surface which is far closer to the gravity field sources in the Earth crust responsible for gravity field variations in the 5-100 km wavelength.

The height of the oceans closely assembles an equipotential surface of gravity and dense observations of the height of the ocean have become an increasing important supplement to traditional terrestrial, ship borne and airborne observations.

Satellite altimetry works conceptually by the satellite transmitting a short pulse of microwave radiation with known power towards the sea surface, where it interacts with it. Part of the signal is returned to the altimeter where the travel time is measured accurately using atomic clocks. Accurate determination of sea surface height from the altimeter range measurement involves a number of corrections: those expressing the behavior of the radar pulse through the atmosphere, and those correcting for sea state and other geophysical signals.

Satellite	Duration	Inclination (degrees)	Repeat times (days)	Track distance at Equator (km)	noise (m)
Geosat	1984-1988	108	~3, 17	4, 150	0.07
ERS-1	1991-1996	98	3,35,356	900, 75, 8	0.06
ERS-2	1995-2006	98	35	75	0.05
TOPEX/Poseidon	1992-2006	66	~9.9156	315	0.04
Jason-1	2002-2008	66	~9.9156	315	0.03
Jason-2	2008 ->	66	~9.9156	315	0.03
GFO	2001-2008	108	17	150	0.06
Envisat	2001 ->	98	35	75	0.04
ICESat	2002 ->	94	90	‘110’	0.04
Cryosat-2	2010 ->	88	369	7	0.01

Table 9.1 Specifications for recent and ongoing satellite missions carrying altimeters.

During the design of a satellite mission one of the first steps is to make a decision of how the satellite is flown and how the orbital parameters are defined (e.g., inclination with respect to the Equator and repeat time). This will define the observational pattern of the satellite given by the ground track distance in Table 9.1 and also shown in Figure 9.1, where the denser ground tracks is preferred for recovering high resolution marine gravity. The inclination in Table 9.1also determines the maximum latitude covered by the satellites. All altimetric satellites leave a polar gap of different size which stresses the importance of recovering gravity in the Polar Regions through project like the Arctic Gravity field (ArcGP) project (Kenyon and Forsberg, 2008). An inspection of the different inclinations in Table 9.1 reveals, that the ERS and Envisat satellites leave smaller polar gap than the TOPEX/Poseidon, Jason, Geosat and GFO. ICESat laser mission leaves a polar gap with a radius of 400 km and the newly launched Cryosat-2 leaves a polar gap with only 200 km.

Data from satellite altimeters are available as either exact repeat mission (ERM) in which the sea surface height observations are being repeated at regular intervals at a low spatial resolution. Such design is very important for oceanography and climate science, but not applicable for high resolution gravity field modelling at least for its stationary part. The geodetic mission (GM) data are far more interesting for geodesy. In the GM the satellite flies in a non-repeating orbit or an orbit with a very long repeat and hence, the sea surface height observations are only taken once at each location but at a much higher spatial density. Consequently, this configuration creates a much denser mesh of observations as shown in Figure 9.1.

During the last twenty years or so, the six eight satellites carrying altimeters (Geosat, GFO, ERS-1, ERS-2, Envisat, TOPEX/POSEIDON, Jason-1 and Jason-2) have recorded more than 60 years of ERM observations (over a period of 25 years), whereas less than 2.5 years of GM altimetry have been recorded. The only two geodetic missions were performed by the ERS-1 and Geosat satellites. During 199 the ERS-1 performed two interleaved repeats of 168 days resulting in a uniform global dataset having 7 km along track resolution and 8 km across track resolution at the Equator. The Geosat GM lasted 1.5 years during 1985 and 1986. However, these data were not declassified by the US navy until 1995. The Geosat GM did not have a constant across track distance, as Geosat was put in a drifting ~3-day orbit during the GM. A total of 35 million altimetric sea surface height observations with an average track distance of 6 km at the Equator are available from this mission within the +/- 72°parallels. Examples of the ground track pattern measured by the TOPEX & Jason-1 ERM; ERS and Envisat ERM; Geosat ERM and ERS-1 ERM are shown in Figure 9.1.

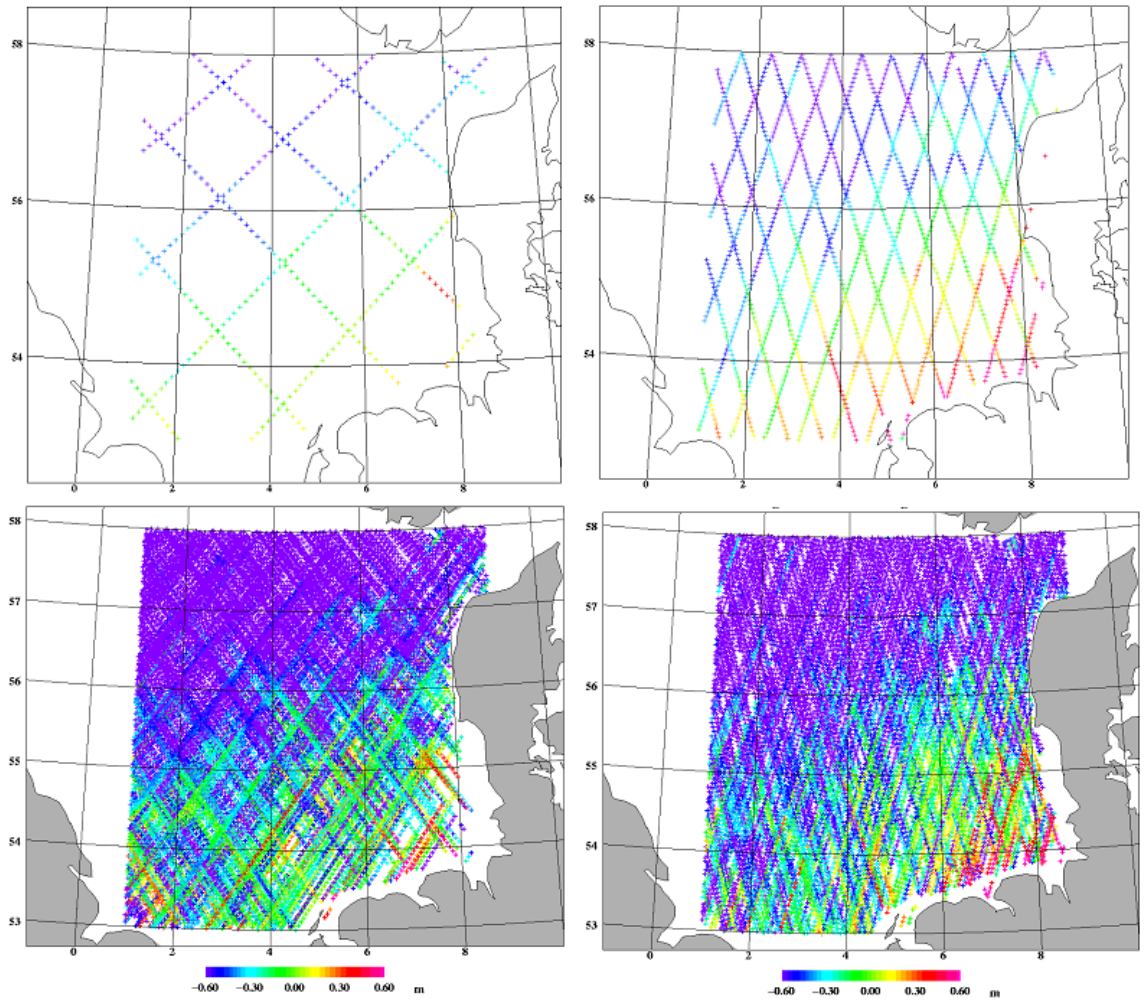

Figure 9.1. Ground tracks patterns in the North Sea for Exact Repeat Missions (upper) versus Geodetic Missions (lower). The TOPEX/Poseidon and Jason satellites (upper left); ERS-1, ERS-2 and Envisat ERM (upper right); Geosat GM (lower left), and ERS-1 GM (lower right).

The major problem for the recovery of high resolution gravity is the fact that only the old and relatively in-accurate GM data (compared with present day altimeters) have adequate spatial resolution. Consequently the geodetic community has made every effort possible in order to enhance the quality and the resolution of the GM data. This is because the accuracy of the derived gravity field is directly proportional to the accuracy with which the sea surface height can be determined.

Sea surface height accuracy has been improved dramatically over the last decade through a reanalysis of the old data applying a technique called retracking. Retracking describes the way a mathematical model is fitted to the returned power from the sea surface also called the waveform. From the parameters derived to fit the chosen mathematical model the sea surface height is derived. Below retracking is briefly introduced for interested readers.

9.2 Retracking

Over the ocean the power returned from the sea surface has a characteristic waveform shape as a function of time which was mathematically described by Brown (1977), and this general form has since been called a Brown waveform. A total of six parameters can be seen to determine the waveform as shown in Figure 9.2. These are: the epoch time at mid height, the trailing edge slope, the leading edge slope, the skewness, the thermal noise (P_0) and the amplitude of the signal (P).

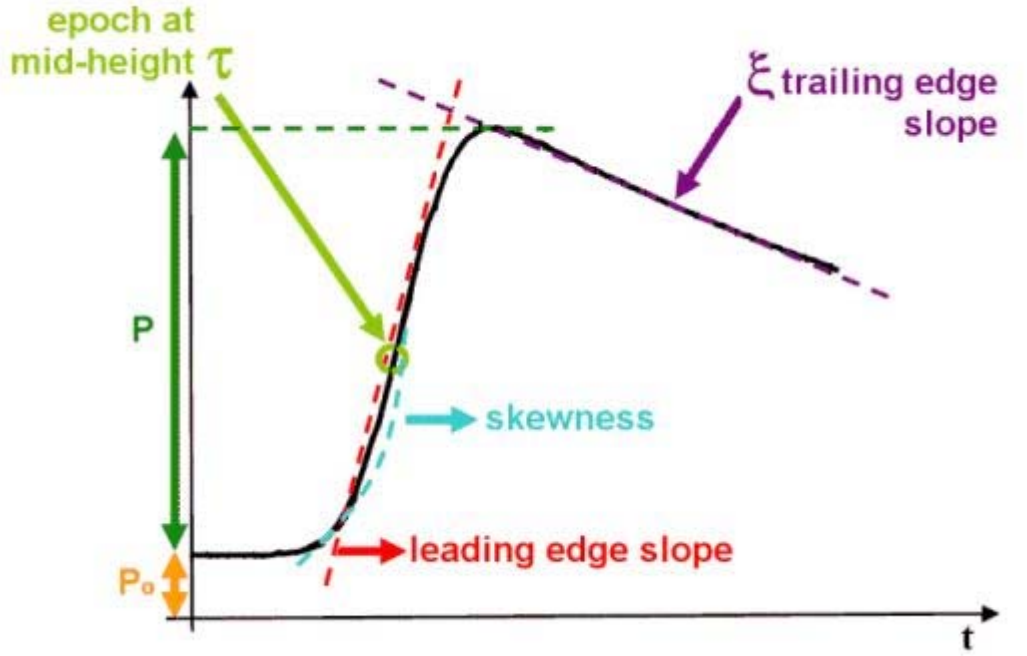

Figure 9.2 The returned power as a function of recording time for a typical altimetric observation over the ocean modeled as a Brown waveform. The figure has been modified from ESA (www.esa.int)

The epoch time at mid height where the waveform have risen to half its full power, is defined to determine the exact time of the return pulse defining the height of the sea surface (by multiplying with the speed of the radar pulse and dividing by 2 for the return of he signal). The 'leading edge slope' reflects the scattering of the radar signal by the sea surface. Higher waves will create more uniform distribution of the returned

power and consequently, the 'leading edge slope' will be low. In the opposite situation where the surface is flat (acting like a mirror) the power will be returned instantly, and the leading edge and trailing edge slopes will be nearly vertical.

Maus et al. (1998) pointed out that in the least squares estimation of the six parameters defining the Brown waveform, the correlation between the 'leading edge slope' and the epoch time is very high. This leads to the development of a secondary re-analyzing of the waveform data through re-tracking (also called repicking) of each 18 Hz individual waveforms. In this secondary run the leading edge slope or equivalently the significant wave height is fixed from the first re-tracking run through smoothing and the estimation can be limited to a few parameters which result in a much more robust and smooth sea surface height estimation as shown in Figure 9.2. This proved to be particularly important particularly for the ERS-1 data where the thermal noise (P_0) is suppressed.

The second important finding was the fact that between 6-9 % of the (ERS-1) data are rejected globally by the Brown retracker applied by the space agencies, as their retracker proved to be too restrictive. This leads to the development of a suite of more tolerant retrackers by Berry et al. (2005) to account for reflections from various surfaces. This later proved to be particularly important in coastal and polar region where the percentage of non-Brown waveforms increases dramatically (Andersen et al. 2010). This increased the number of altimetric observations significantly as also shown later in Figure 9.27. This development will be further described in section 9.13.4, as a major contributor to the improvement of high resolution global marine gravity field modeling over the last 10 years can be directly associated with retracking and improved accuracy of sea surface height estimation.

9.3 Sea surface height observations

Altimeter data are distributed through agencies like, EUMETSAT, AVISO, PO.DAAC and NOAA. In addition to these operational data centers, the Radar Altimeter Database System (RADS) delivers harmonized, validated and cross-calibrated sea level database from all altimetric missions.

The altimeter measures the range to the sea surface and the (retracked) altimetric range observations are initially corrected for a number of range corrections to model the behavior of the speed of the radar pulse (speed of light) through the atmosphere. The range corrections also accounts for the interaction with the sea surface through the sea state correction (e.g., Andersen and Scharroo 2009; Fu and Cazenave 2001). The height of the spacecraft is determined relative to the reference ellipsoid through Precise Orbit Determination and more recently including GPS (Fu and Cazenave, 2001). Combining the knowledge of the height of the spacecraft with the corrected range gives the sea surface height relative to the reference ellipsoid as also shown in Figure 9.3. The sea surface height h can, in its most simple form, be described according to the following expression

$$h = N + \zeta + e \qquad (9.1)$$

Where N *i*s the geoid height above the reference ellipsoid, ζ is the time-variable sea surface topography, and e is the error.

In geodesy the geoid N (or the geoid slope) is the important signal. In oceanography the sea surface topography ζ is of prime interest.

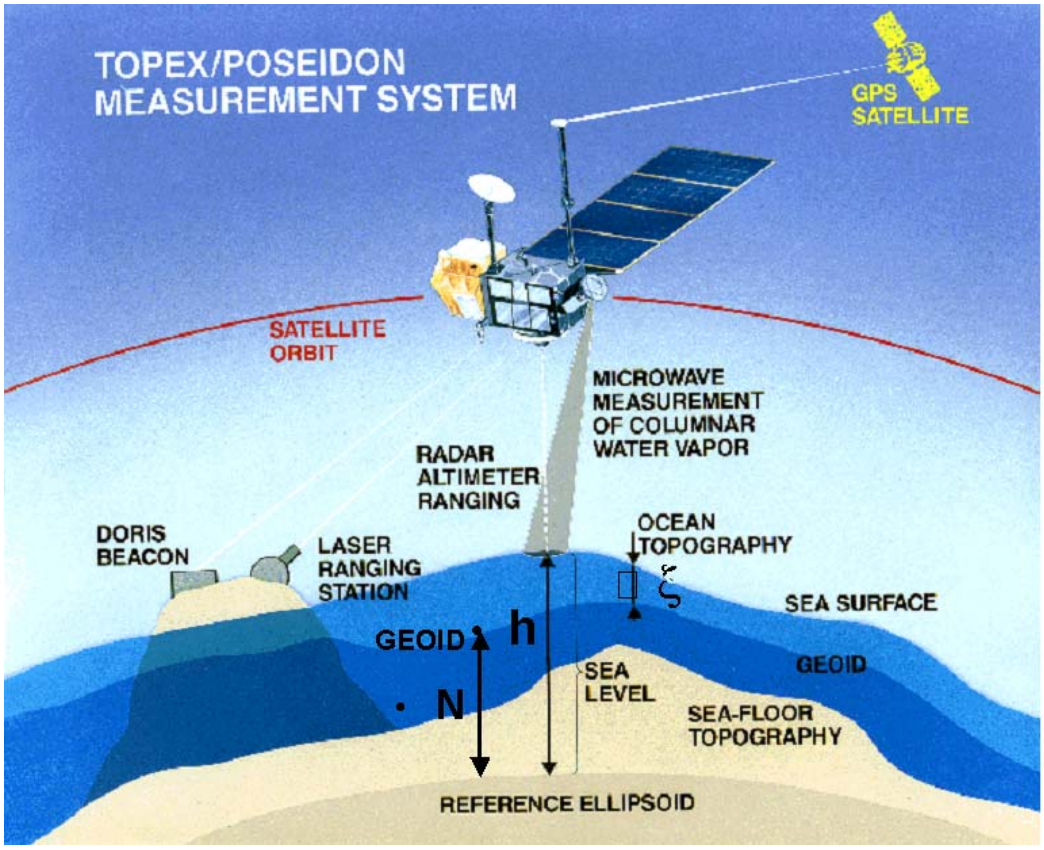

Figure 9.3 Schematic illustration of the satellite altimeter measuring principle. The sea surface height (h) relative to the reference ellipsoid is the sum of the Geoid N and ocean topography. Figure modified from AVISO.

The geoid N can be described in terms of a long wavelength reference geoid N_{REF}, and residuals ΔN to this. Similarly the sea surface topography can be described in terms of a mean dynamic topography (ζ_{MDT}) and a time varying sea surface topography ($\zeta(t)$) also called the dynamic ocean topography (DOT). Normally the largest contributors to the time varying sea surface topography ($\zeta(t)$) are removed as part of the standard set of geophysical corrections. These include the tidal correction and the dynamic atmosphere correction. The ocean tide correction is responsible for more than 75% of the total signal variance (Ray et al. 1991). The dynamic atmosphere account for less than 10% of the total signal variance and include a correction for the atmospheric pressure effect, as the sea level react as a huge inverted barometer coming up with the atmospheric pressure is low and going down when the pressure is high.
This way the time varying sea surface topography ($\zeta(t)$) will only contain contributions from primarily wind and other high frequency effects. Sea surface height can then be written like:

$$h = N_{REF} + \Delta N + \zeta_{MDT} + \zeta(t) + e \qquad (9.2)$$

The interesting quantity for gravity field modeling is the residual geoid height ΔN. The accuracy with which this quantity can be determined is directly related to the accuracy with which the other contributors in equation (9.2) can be determined. Consequently, it is important to model and remove these as accurately as possible which is the focus of the subsequent section.

Assuming that N_{REF}, ζ_{MDT} and $\zeta(t)$ are all of long wavelength characters then these are almost identical between two neighbouring altimetric point (h_i,h_j) some kilometres apart. Consequently the difference becomes equal to the slope of the residual geoid signal along the altimeter track like

$$h_i - h_j \approx \Delta N_i - \Delta N_j + e \approx \partial N + e \qquad (9.3)$$

The geoid slopes is closely related to the deflections of the vertical (DOV) in the north and east direction called (ξ, η) as defined in (2.101) and later in this chapter their use with altimetry will be described in detail.

The major argument of using DOV rather than geoid heights is the fact that DOV values are less contaminated by long-wavelength errors as will be demonstrated easier to process as the user does not need to go to model and remove long wavelength signals and particularly the time-variable dynamic sea surface topography ($\zeta(t)$.

There are, however two drawbacks of using slopes compared with direct height observations. The first stems from the inclination of the satellites (108° and 98° for Geosat and ERS, respectively). This means, that at low latitudes the geoid slope in the north-south direction is derived much more accurately, than the east-west slope. Similarly the north-south-slope is less accurate derived at the turning latitudes of the satellites (se Sandwell and Smith 1997 for details). The second drawback is the fact that in shallow water regions, the spatial scales of the time-variable dynamic topography ($\zeta(t)$) is scaled down with the square root of the depth and also amplified and the assumption that this quantity is identical from one altimetric observations to the next becomes questionably and the noise *e* is increased.

To get from along track slopes in (9.3) to DOV in the north and eastern directions several possibilities exist. By definition the along-track DOV called ∂h below defined as the along-track gradient of the geoid (with opposite sign) along the track given like

$$\partial h = -\frac{\partial N}{\partial s} \qquad (9.4)$$

with *s* being the along track distance. Consequently a gridded geoid surface is needed. This can be created from e.g., a cubic spline fit to the along track altimetric geoid height data. Then the along track derivative is obtained by differentiating the spline. This approach, however, gives noisy DOV due to the interpolation error of the spline.

A better result is obtained by approximating the along-track DOV by the slope of two successive geoid heights.

$$\partial h \cong -\frac{N_2 - N_1}{d} \qquad (9.5)$$

where *d* is the along track point spacing and the location of ∂h is the mean location of the two points. In order to derive the northern and eastern DOV from the along track DOV the following equation system is set up to determine these using several points in a small cell (cf. sec. 1.9)

$$\partial h_i + v_i = \xi \cos\alpha_i + \eta \sin\alpha_i \qquad i = 1,...,n \qquad (9.6)$$

where v_i is the residual, α_i is the azimuth of ∂h_i, n is the number of points and (ξ,η) is the north and east component of the DOV. It must be noticed that the along-track DOV from different satellite mission and at different latitudes have different azimuth, which complicate the use of (9.6) for resolving gridded northern and eastern DOV from along-track DOV.
At crossover location where one north going track crosses a south going track, the north and east components of the DOV can be directly derived from the two along track DOV observations. This gives far better determination of the slopes. However crossover locations are infrequently spaced. A thorough description of the individual steps in the method is given by Hwang et al. (2002)

9.3.1 Mean sea surface and mean dynamic topography

In a perfect world altimetric observations would be available over infinite time. This would mean, that the dynamic topography $\zeta(t)$ average out from repeated observations along exact repeated ground tracks making ($\zeta(t) = 0$) in (9.2). The surface defined by the repeated satellite observations would then be the mean sea surface (h_{MSS}), which is the sum of the geoid height N and the mean dynamic topography (ζ_{MDT}). This way (9.2) reduces to

$$h_{MSS} = N + \zeta_{MDT} + e \quad = N_{REF} + \Delta N + \zeta_{MDT} + e \qquad (9.7)$$

In case a "perfect" MSS with adequate resolutions existed then ΔN could be determined directly from this model. Present day MSS models like DNSC08MSS are derived using the most accurate filtering of the temporal sea surface variability with a limited time span and simultaneously obtaining the highest spatial resolution. This is normally achieved by combining data from the highly accurate exact repeat mission (ERM), with data from the older non-repeating geodetic mission (GM) like ERS-1 and Geosat.
This also means that in between the repeat tracks the mean sea surface is only determined by the GM data. In order to obtain the "best" high resolution marine gravity field experiments have shown that it is better to use the remove-restore of the geoid signal and crossover adjustment on individual tracks as proposed in the subsequent sections without applying the MSS.

The mean dynamic topography (MDT) is the quantity bridging the geoid and the MSS and the quantity constraining large scale ocean circulation. This equations also state, that a better estimation of the geoid and altimetric MSS is, in particular, expected to improve the determination of the mean ocean circulation (Wunsch 1993).

The MDT has long wavelength character and ranges between +/- 1.8 meter as shown in Figure 9.4 with highest values around the Equator and lowest values towards the poles which shows that a major part of the MDT is due to thermal expansion in the upper layer of the ocean.

In order to derive gravity from residual geoid signal it is important to remove the MDT contribution from the MSS as mentioned in (9.2). Failure to do this will introduce a false gravity signal in the altimetric derived gravity signal. The lower part of Figure 9.4 shows exactly this effect from failure to account for the effect of the MDT. The false gravity signal ranges up to 3-5 mGal in the large current regions even though the figure only shows the smoothed gravity effect ranging up to 2 mGal.

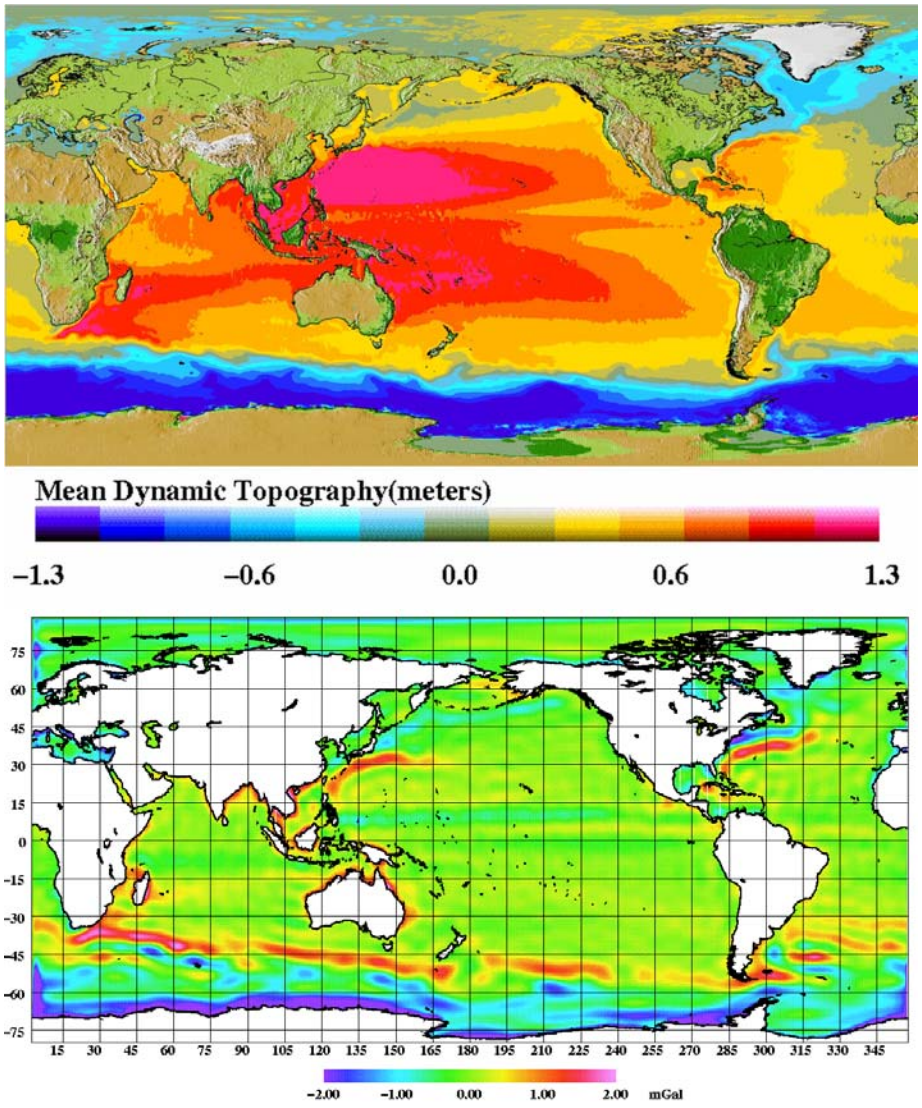

Figure 9.4. The Mean dynamic topography (upper figure) and the false gravity signal (lower figure) caused by the mean dynamic topography (PGM07A) if this is not removed from the sea surface height observations prior to gravity field determination.

9.3.2 Remove-restore for satellite altimetry

The use of remove restore technique is extremely important for the efficient computation of short wavelength gravity field using altimetric sea surface height data. By removing a known reference geoid model (e.g. EGM96 or EGM2008) a residual geoid field is obtained, which is statistically more homogeneous and smoother than the total field. The removal of a reference field has the effect, that gravity field information outside the data-area is implicitly accounted for and the covariance functions will have smaller correlation distance (Part II, eq. 2.82). Therefore the computation can be carried out in smaller a region.

Along with the reference geoid the mean dynamic topography (ζ_{MDT}) must also be removed as described above. This gives the residual sea surface height h_{res} from (9.2) like

$$h_{res} \approx \Delta N + \zeta(t) + e \qquad (9.8)$$

It is important to be aware of how much signal is removed along with the remove/restore of the geoid signal. This will be a function of the accuracy of the geoid as well as the degree and order used for the spherical harmonic expansion. An example of this is the new EGM2008 geoid (Pavlis, ibid) which removes signal up to spherical harmonic degree and order 2160. This is far more than most other geoid model like EGM96, GGM02, EIGEN-GL04, which only models geoid signal up to spherical harmonic degree and order 360, 200 and 150, respectively.

The residual signal can e.g. be evaluated using the Tscherning/Rapp degree variance model (Tscherning and Rapp 1974)

$$\sigma_i^{TT} = \begin{Bmatrix} \kappa_i & i = 2,.....,2160 \\ \dfrac{A}{(i-1)(i-2)(i+4)}\left(\dfrac{R_B}{R}\right)^{i+1} & i = 2161..... \end{Bmatrix} \qquad (9.9)$$

where the Bjerhammer radius R_B = R-7 km and R is the radius of the Earth, A = 1571496 m^4/s^4, i is the degree and κ_i is the error degree variance of EGM2008.

Evaluating (9.9) gives a residual geoid signal of 4-5 cm and a correlation length of 7-9 km once EGM2008 has been removed up to degree and order 2160. This compares to a residual signal of 30-40 cm and correlation length of 20-25 km for the EGM96 geoid model complete up to degree and order 360.

9.3.3 Dynamic sea surface topography

The amplitude of the dynamic sea surface topography $\zeta(t)$ - recalling that ocean tides and atmospheric pressure have been removed - will be largest in the major current systems such as the Gulf Stream, the Kuroshio Extension in the Pacific Ocean, the Antarctic Circumpolar Current, and in the coastal regions as seen in Figure 9.5.

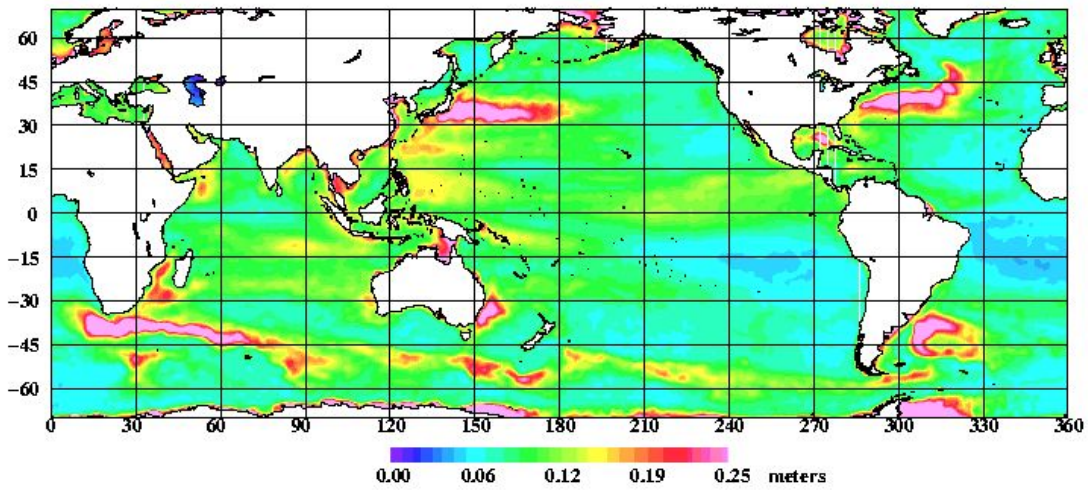

Figure 9.5 Standard deviation of the timevarying dynamic sea surface topography from 6 years of Envisat altimetry.

Data from repeated ERM like T/P, JASON1+2, GFO, ERS-2 and Envisat efficiently average out the dynamic sea surface topography through multiple observations at the same locations. However, the ground track spacing of these satellites (>75 km) does not enable adequate resolution for retrieving the high resolution gravity field. In non-repeating geodetic mission data the sea surface height observations are observed once and consequently measures must be taken to remove the dynamic sea surface topography that will otherwise contaminate the residual geoid height signal.

The dynamic sea surface topography $\xi(t)$ are mainly caused by wind, waves and pressure *and* generally has a long wavelength characters with wavelength longer than 100-200 km. Failure to remove this signal will create along track stripes in the derived gravity field known as the "orange skin" effect after the texture of an orange. The effect on one of the first altimetric mean sea surfaces is illustrated in Figure 9.6.

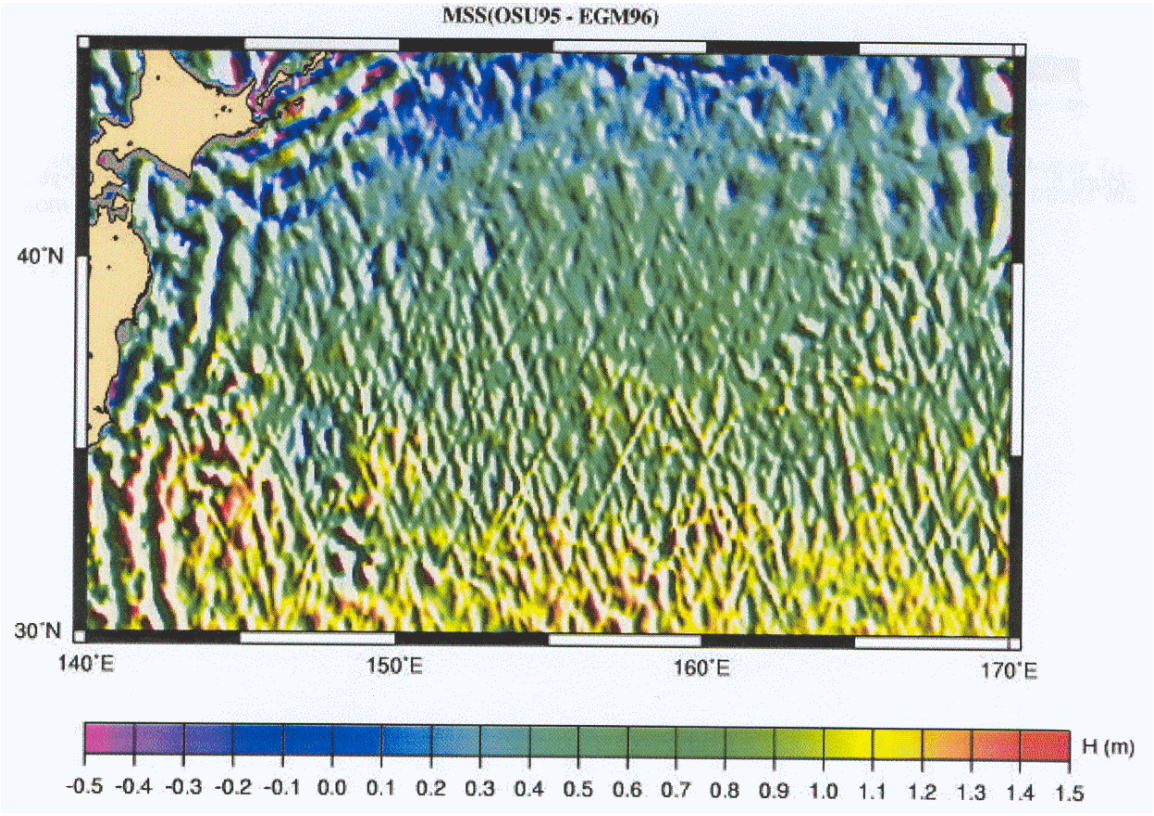

Figure 9.6. The "orange skin" effect in the Kuroshio Extension in the Pacific Ocean from un-modelled dynamic sea surface topography. The picture shows the OSU95 mean sea surface (Yi 1995) relative to EGM96 (after Hernandez and Schaeffer 2000). The same orange skin effect will be visible if gravity is derived from these data.

Erroneous track related "orange skin" signal will result in large along track gravity field errors. One way of avoiding this is to use DOV values in stead of heights as stated previously.

Another way is so use sea surface height observations but to perform a cross over adjustment on the data. A cross-over adjustment uses the fact that the geoid residuals should be identical at all locations where ascending tracks cross descending tracks hereby mutually adjusting the tracks to limit track related errors. The cross-over adjustment is the subject of section 9.4.

9.4 Crossover adjustment

In order to remove the dynamic topography on particularly non-repeating geodetic mission tracks from the ERS-1 and Geosat missions a crossover adjustment is applied. The location where a descending track intersects an ascending track is called the single satellite crossover location. Altimetric satellites are designed to create a fine interweaved net of tracks and diamonds for the use of orbit computation (se figure 9.1) and for GM missions this mesh is extremely fine. The crossover adjustment is carried out to limit track related errors and other long wavelength errors by minimizing height differences at crossover location between ascending and descending tracks.

The motivation for performing crossover adjustment is the assumption that the geoid signal is stationary at each location. With the launch of GRACE temporal geoid variations have been demonstrated (e.g., Chambers et al. 2007), but these are extremely small, and for the current investigation it can be assumed that the geoid is static.

Consequently the geoid height should be the same on ascending and descending tracks at crossing locations. On the contrary dynamic sea level signals should be different. Crossover discrepancies are computed as differences in sea surface heights between observations on north and south going tracks, like $d_{ij}=h_i-h_j$.

For very short arcs the track related errors can be modelled by a constant bias terms for each track, then

$$h_i - h_j = a_i - a_j + v_{ij} \qquad (9.10)$$

where $(a_i, a_j,)$ are the unknown bias parameters related to the north and south-going track and v_{ij} are the residuals. On matrix form, this observation equation takes the form $\underline{d}= A\underline{x} + \underline{v}$, where $\underline{x}$ is a vector containing the unknown bias parameters. These are then estimated in a least squares adjustment (e.g. by minimizing the residuals, v_{ij}) like

$$\underline{x} =(A^T C_d^{-1} A + cc^T)^{-1} A^T C_c^{-1} \underline{d} \qquad (9.11)$$

The equation system has a rank deficiency of one, so a constraint is needed. The constraint **c**, used is normally that the mean value of the biases should be zero, $\mathbf{c}^T\underline{x}=0$. (Knudsen, 1993)

For medium length arcs (e.g., shorter than 2000 km) the track related errors can be modelled by bias and tilt terms. Then the residuals, v_{ij}, are minimized in a least squares adjustment of

$$h_i - h_j = (a_i + b_i\mu_j) - (a_j + b_j\mu_i) + v_{ij} \qquad (9.12)$$

For longer arcs (e.g., longer than 2000 km) the track related errors are not conveniently modelled using linear models (bias + tilt) but must be modelled using cosines and sine terms like

$$h_i - h_j = (a_i + c_i \sin\mu_j + d_i \cos\mu_j) - (a_j + c_j \sin\mu_i + d_j \cos\mu_i) + v_{ij} \qquad (9.13)$$

where (h_i-h_j) is a cross-over difference and $(a_i, b_i, c_i\ d_i, a_j, b_j, c_j.\ d_j)$ are the unknown bias, tilt and higher order parameters. μ_j and μ_i are the coordinates along the i'th and the

j'th track of the cross-over points of the j'th and i'th track respectively. Here once could use orbital angles (true anomaly) times or longitudes coordinates but these are not exactly linear function of one another.

After remove the reference geoid (EGM96 or EGM2008) only relative short altimetry tracks needs to be investigated as shown in section 9.3.2. Consequently, a crossover adjustment using bias and tilt is adequate. In this case the cross-over adjustment has a rank deficiency of four and the free or unknown surface is described by a bilinear function (Schrama 1989, Knudsen and Brovelli1991):

$$D = s_1 + s_2\mu_j + s_3\mu_i + s_4\mu_j\mu_i \qquad (9.14)$$

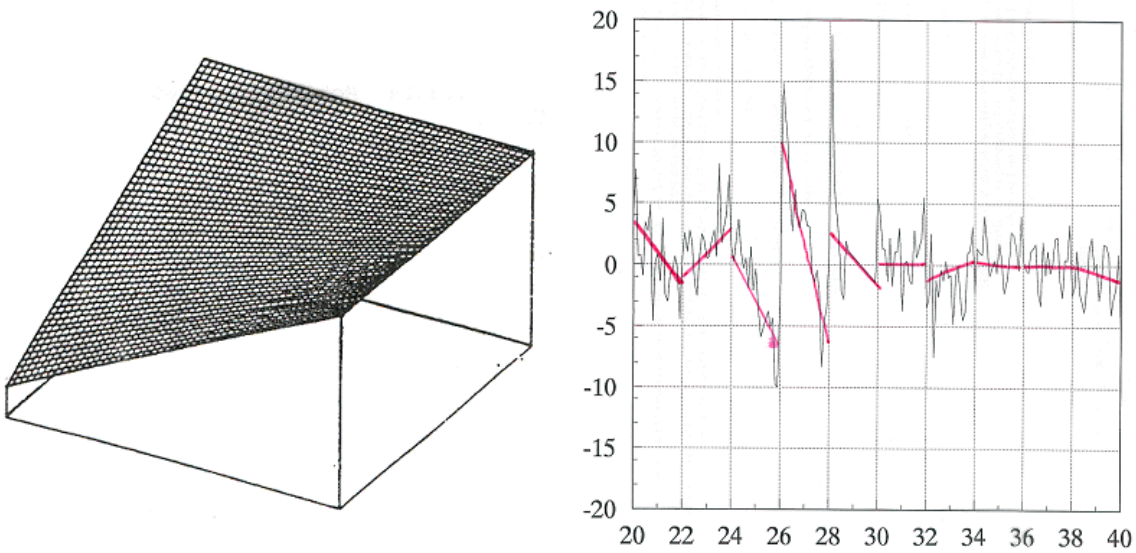

Figure 9.7 *Left. Illustration of the free surface in a bias and tilt crossover adjustment. Right: Gravity difference (mGal) along neighbouring areas of independent crossover adjustments for the KMS98 gravity field crossing the Hawaiian chain along 180°E. The block sizes used for the crossover adjustment is 2° latitude by 10° longitude with a 1° boundary in the computation.*

The rank deficiency problem is illustrated in Figure 9.7 for a free surface in a bias and tilt cross-over adjustment. The problem may be solved by fixing two parallel tracks (Rummel 1993). Then two "master" tracks have to be selected, what can be difficult, since criteria for judging some tracks better than others are needed (here ERM tracks can be used). Normally, it is more attractive to do a "free cross-over adjustment" by applying a constraint that minimizes the free surface, eq. (9.12), so the solution projected on the null space is zero. Such a constraint is given by Knudsen and Brovelli (1991) where a week minimum variance constraint is used.

Occasionally, the combined effect of removing the mean dynamic topography ξ_{MDT} and the free surface is that the altimetric surface does not have zero mean after the crossover adjustment, even if the area of computation is larger than the wavelengths included in the geoid model removed during the processing of the data. It may be corrected by re-estimating the parameter, s_1, s_2, s_3, and s_4, of the free surface, (9.14), and removing them from the data. The drawback is that some long wavelength parts of the residual geoid are removed. Hence, the altimeter observations will only represent

the relatively short wavelength parts of the geoid residuals, δN, and the time-variable dynamic topography, $\delta\xi$, that is

$$h^c = \delta N + \delta\xi + v \qquad (9.15)$$

The deviations between the altimeter data and the geoid model may alternatively be removed before the crossover adjustment by fitting each of the individual tracks to the geoid model. Again using a bias and a tilt for each track this may be carried out in a least squares adjustment minimizing the residuals, V_{ik}, along the i 'th track. That is

$$h_k = a_i^o + b_i^o \mu_k + V_{ik} \qquad (9.16)$$

The residuals, V_{ik}, contain geoid and stationary SST of wavelengths shorter than the length of the i'th track. For sufficiently long tracks the residuals may be used as geoid height observations. However, the cross-over discrepancies have not been minimized.

A joint fitting of the tracks to a geoid model and an adjustment of the cross-over discrepancies can be obtained by minimizing the residuals, v_{ij} and V_{ik} in (9.12) and (9.16), simultaneously (e.g. $a_i = a^o{}_i$ and $b_i = b^o{}_i$). In that case no rank deficiency and subsequent free surface problems exist, but relative weights of the residuals have to be determined in order to obtain satisfactory results. Hence, if a relative weight, w, is applied on the residuals in (9.16), an adjustment of the following expression is carried out:

$$\sum v_{ij}^2 + w \sum V_{ij}^2 = \min \qquad (9.17)$$

If the relative weight, w, is small the cross-over discrepancies are primarily minimized; if w is large the individual tracks are primarily fitted to the geoid model.

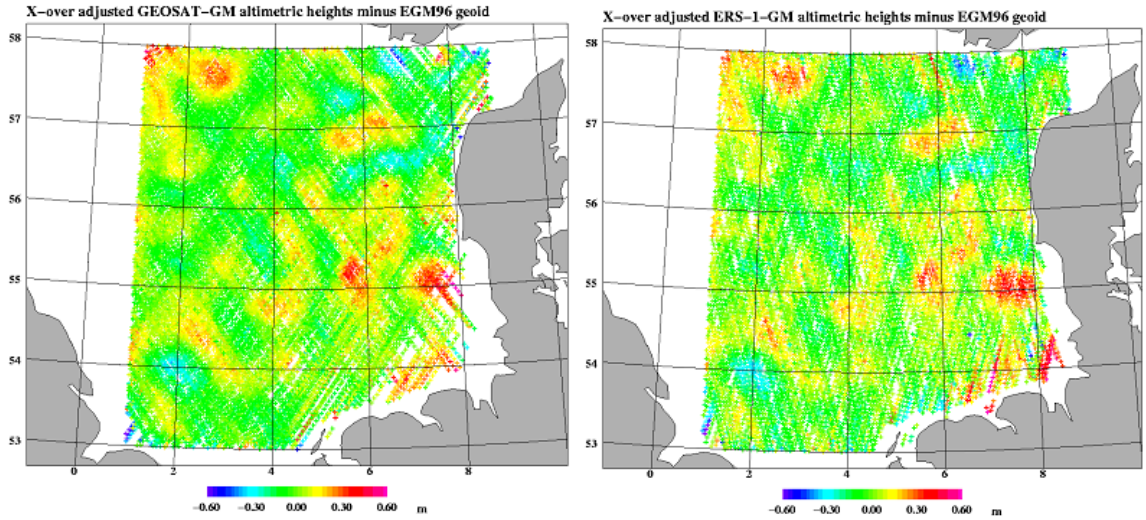

Figure 9.8*. The effect of a crossover adjustment on the Geosat (right) and ERS-1 (left) GM observations shown in Figure 9.1.*

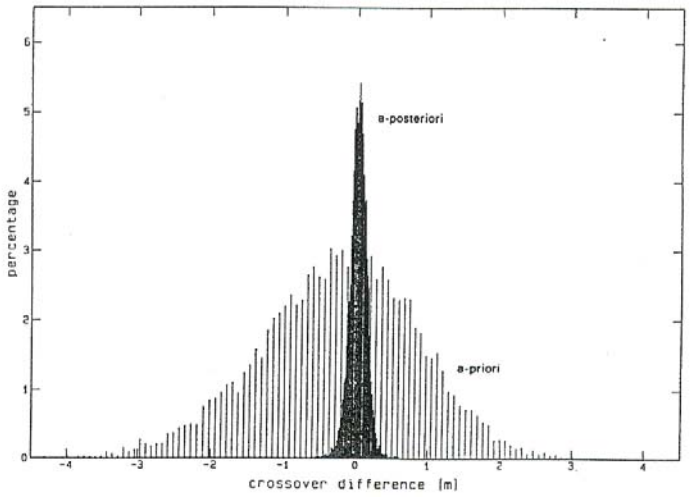

Figure 9.8. *Apriori and a-posteori crossover differences after a crossover adjustment of ERS-1 geodetic mission observations. Figure courtesy of Rummel (1993)*

The effect of a crossover adjustment on the Geosat and ERS-1 geodetic mission observations, shown in Figure 9.8, in a test example in the North Sea with illustration of the statistics of the effect of a-priori differences after a crossover adjustment, shown in Figure 9.9. The original Geosat and ERS-1 GM data prior to crossover adjustment is shown in Figure 9.1. Notice that the colour scale for Figure 9.1 and 9.8 is the same. The North Sea is known for very large dynamic sea surface topography signal. The crossover adjustment was carried out on the Geosat and ERS-1 independently and the resulting crossover adjusted picture shows a high degree of agreement between the two datasets. The comparison confirms that the residual signal is a consistent signal in both datasets and that the crossover adjustment has efficiently removed the dynamic ocean surface topography which leaves only the following signal in the residual sea surface height

$$h_{res} \approx \Delta N + e \qquad (9.18)$$

A careful inspection of Figure 9.8 reveals that the two datasets are not completely identical and some small differences still remain. The differences are typically outliers that can be picked up by the editing procedure described below, but also some residual track related signal can be seen.

The various steps described in this and the preceding sections have efficiently removed a reference geoid signal, the mean dynamic topography, and the time variable sea surface height signal in the geodetic mission data. This way, only the residual geoid signal remains in the altimetric sea surface height observations. This data will be used to derive global high resolution marine gravity field in the next sections. However, prior to that it is important to describe the data editing and the error-budget of the sea surface height data as well as the huge improvement in data quality achieved through retracking the last 5-10 years.

9.5 Data editing, data quality and error-budget

The quality of the derived high resolution gravity field is fundamentally dependent on the accuracy of the sea surface height observations and it is important to be aware of the accuracy of the input data as well as to carry out careful editing of the data.

All altimetric data have been edited for gross errors by the space agencies and the data distribution centres like AVISO, PODAAC or RADS. However, errors still remain due to wrong processing (e.g., retracking and wrong corrections), as well environmental errors like the presence of sea ice or coast. These errors frequently require more sophisticated methods to detect and remove.

Most outliers can be edited out by using standard editing criteria on the following information associated with the satellite altimetry data. All range and environment corrections should be present and within certain thresholds. The sea surface height and slope should be below a certain threshold.

As threshold either global numbers or local numbers based on the local conditions can be used (i.e, Hwang et al. 2003). One example of local conditional error removal technique is the technique used for the derivation of the DNSC08 global marine gravity field. This editing was applied on the residual geoid heights after the removal of dynamic topography (crossover adjustment). This editing technique uses an efficient iterative de-spiking routine in which each altimetric observation is compared with the interpolated value from the nearest 64 points. For the interpolation a correlations length of 20 km is applied to slightly smooth interpolation. If the point departs from the interpolated value by more than 2.5 times the standard deviation of the 64 local points the point is removed. This process was repeated iteratively using the reduced dataset until no further data points were removed. This was normally achieved in 3-5 iterations and generally removed between 3% and 6% of the altimetric sea surface height observations.

The main contributors to the errors e on the individual altimetric observations are the following:

$$e = e_{orbit} + e_{tides} + e_{range} + e_{retrack} + e_{environment} + e_{noise} \tag{9.19}$$

where

e_{orbit} is the radial orbit error
e_{tides} is the error due to residual tidal signal
e_{range} is the error on the range correction.
e_{retrak} is the error due to retracking
$e_{environment}$ is the error due to the presence of sea ice or coast
e_{noise} is the measurement noise.

For the use of DOV, the error on sea surface slopes must be derived. These are found from

$$e_{21} = \frac{\sqrt{e_1^2 + e_2^2}}{d} \tag{9.20}$$

Where e_1 and e_2 are the standard deviation on the consecutive sea surface height observations h_1 and h_2, and d is the distance.

For the un-retracked ERS-1 GM satellite altimetry, the error budget sums up to around 5-8 cm RMS (Scharroo, personal communication). This is roughly the same for the Geosat (Chelton et al. 1987). The error due to remaining tidal signal will increase in shallow water regions where the applied models are known to degrade (Andersen and Scharroo 2010). The various errors will be addressed more carefully in section 9.11 which focuses on accuracy improvement. The error budget is naturally smaller than the sum of the errors in the applied models through the crossover

adjustment which will removes long wavelength "errors" as well as long wavelength signal.

Figure 9.10 shows the huge improvement in the accuracy of sea surface slopes from retracking. The figure is courtesy of David Sandwell and shows the sea surface slope along six repeated ERS-1 profiles crossing the south Pacific with both high and low significant wave-heights. Slope errors were calculated using the 18Hz measurements and slightly low pass filtering. A slope error of 1 μ-rad generally translate into a gravity error of 1 mGal (Sandwell and Smith, 2005), so the retracking algorithm reduces the RMS error by 62% compared with the RMS error for the standard un-retracked data which corresponds to a 38 per cent improvement in range precision (Sandwell and Smith, 2005; Deng et al., 2003)

Improvement in the height or slope accuracy through retracking directly translates into an improvement in both the accuracy but also of the resolution of the obtained gravity field. The higher accuracy of the sea surface height data means that the derived gravity field can be smoothed less, which again means that higher frequencies are retained in the derived gravity field. This was also demonstrated by Andersen et al. (2009)

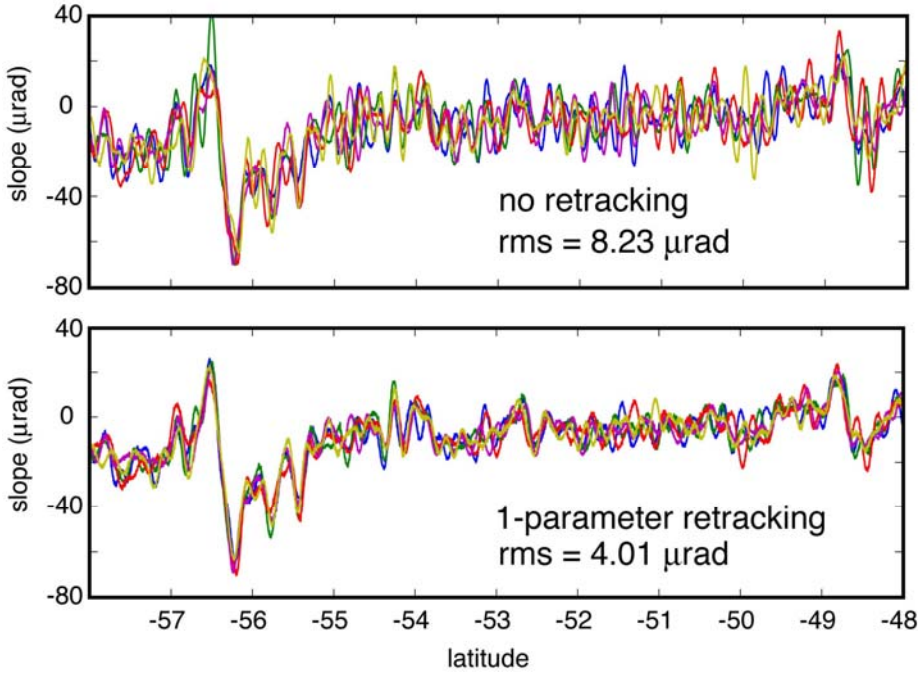

Figure 9.10 *Six repeated along-track sea surface slope profiles in the South Pacific Ocean. Upper profile is derived from the onboard tracker available in the waveform data record (RMS = 8.23 μrad). Lower profiles have been derived from a 1-parameter retracking algorithm constrained by smoothing the rise-time and amplitude parameters as in the text (RMS = 4.01 μrad). Figure courtesy of David Sandwell.*

In many ways the ability to squeeze out more accurate gravity field information from retracking and reprocessing existing ERS-1 and Geosat GM datasets are close to being exhausted.

Fortunately, there are several new datasets coming in the near future which will bring a huge improvement in data accuracy, coverage and quality. The Cryosat-2 will firstly improve the coverage of the Arctic Ocean as it has an inclination of 88 degrees

bringing it 200 km from the North Pole. Secondly the repeat period is 369 days which gives higher ground track density than even the ERS-1 geodetic mission. Finally, the accuracy of the Delay-Doppler altimeter onboard Cryosat-2 will be a factor 2-3 better than the ERS-1 and Geosat altimeters theoretically bringing it down to 1 cm for 1-Hz data (Jensen and Rainey, 2005).

As for the error budget of the future ESA Sentinel-3 SRAL satellite to be launched around 2014 R. Francis, (personal communication, 2009) quotes a 0.8 cm height accuracy for the Ku-band SAR altimeter for a SWH of 2 meters. The height accuracy values for Cryosat-2 and Sentinel-3 should be compared with the 6 cm height accuracy for the ERS-1 and Geosat GM data so these satellites are expected to bring a quantum leap forward in accuracy of future gravity fields.

Finally, as both Jason-1 and Envisat are getting close to end of mission, there are a possibility that one of these satellites will be placed into a non-repeating geodetic mission for a limited time.

9.6 Gravity recovery from altimetry.

For the use with satellite altimetry it is adequate to use a spherical approximation as described Part 2.5. The short wavelength residual geoid height N signal, isolated from satellite altimetry in the previous sections, can be expressed in terms of a linear functional applied on the anomalous potential T known as Brun's formula (2.36)

$$N = L_N(T) = \frac{T}{\gamma} \qquad (9.21)$$

Where γ is normal gravity and T can be expanded into fully normalized spherical harmonic functions on the surface of a sphere with a radius R like in (Part III, eq. 3.14). The anomalous potential T is a harmonic function satisfying Laplace's equation outside the masses

$$\Delta T = \frac{\partial^2 T}{\partial^2 \varphi} + \frac{\partial^2 T}{\partial^2 \lambda} + \frac{\partial^2 T}{\partial^2 r} = 0 \qquad (9.22)$$

and Poissons equation ($\Delta T = -4\pi\gamma\rho$) inside the masses ($\rho$ is density)

For the gravity anomaly Δg we use the spherical approximation is related to the anomalous potential through the following functional similar to (2.100) like

$$\Delta g = L_{\Delta g}(T) = -\frac{\partial T}{\partial r} - 2\frac{T}{r} \qquad (9.23)$$

This equation is frequently called the fundamental equation of physical geodesy.
Combining (9.23) and (9.21) shows that the gravity anomaly is related to the negative of the geoid slope (∂N) which is the quantity that can be computed from the altimetric sea surface heights.

For deriving gravity from altimetric sea surface slopes the deflections of the vertical (DOV) in the north and east direction (ξ, η) along the spherical unit vectors ($\boldsymbol{e}_\varphi$,$\boldsymbol{e}_\lambda$) can be expressed similar to (1.183) like

$$\vec{\varepsilon} = L_\varepsilon(T) = \eta\vec{e}_\lambda + \xi\vec{e}_\varphi \qquad (9.24)$$

where

$$\xi = -\frac{1}{\gamma r}\frac{\partial T}{\partial \varphi}$$
$$\eta = -\frac{1}{\gamma r \cos(\varphi)}\frac{\partial T}{\partial \lambda} \qquad (9.25)$$

In the derivation of marine gravity from satellite altimetry two approaches are generally used.

One is the stochastic approach which predicts gravity directly from the observations using least-squares collocation (LSC). The major advantage of LSC for marine gravity field prediction is the fact that randomly spaced hybrid type data can be incorporated using statistical information about the errors in the data, and at the same time provide corresponding statistical information about the quality of the output gravity values. The drawback of LSC is the fact that it is very computational intensive, even with present day's computers. This approach is described in section 9.7.

The other approach explores deterministic methods for the solution to Laplace's equation. This method requires global integration for the prediction of gravity in every single prediction point, which calls for huge computations and very fast computational methods. One particularly efficient method is a spectral approximation which requires that data have been interpolated onto a regular grid. This method has been widely used in the determination of global marine gravity during the last decade and is the scope of section 9.8

A hybrid approach in which LSC is used to interpolate the altimetric data points and fast spectral methods are used to evaluate (9.23) has also been widely used for local and global gravity field recovery and will be described in section 9.9.

9.7 Least Squares Collocation for altimetry.

Least Squares Collocation (LSC) can be used to simultaneously determine both the signal and the error components (Wunsch & Zlotnicki 1984, Mazzega & Houry 1989, and Knudsen 1991). The generalised form, which is presented here, has been documented by authors such as Tscherning and Rapp (1974), Rapp (1993) and applied to satellite altimetry by Knudsen (1993).

In its general form the relationship between the observations y_i and the anomalous potential can be written in the form

$$y_i = L_i(T) + e_i \qquad (9.26)$$

where L_i is one of the functionals specified in section 9.6, and e_i is an additive noise.

The gravity anomalies Δg are predicted from residual altimetric geoid anomalies h using the form

$$\Delta g = C_{\Delta g h}(C_{hh} + D_{hh})^{-1} h \qquad (9.27)$$

Alternatively the gravity anomalies are predicted from residual geoid slope ε using

$$\Delta g = C_{\Delta g \varepsilon}(C_{\varepsilon\varepsilon} + D_{\varepsilon\varepsilon})^{-1} \varepsilon \qquad (9.28)$$

An estimate of the *a-posteriori* error covariance of the gravity estimate is

$$\sigma_{\Delta g\Delta g} = C_{\Delta g\Delta g} - C_{\Delta gh}(C_{hh} + D_{hh})^{-1} C_{\Delta gh}{}^{T} \qquad (9.29)$$

or for residual geoid slopes

$$\sigma_{\Delta g\Delta g} = C_{\Delta g\Delta g} - C_{\Delta g\varepsilon}(C_{\varepsilon\varepsilon} + D_{\varepsilon\varepsilon})^{-1} C_{\Delta g\varepsilon}{}^{T} \qquad (9.30)$$

where the covariance matrices C_{hh} , $C_{\Delta gh}$, $C_{\Delta g\Delta g}$, $C_{\varepsilon\varepsilon}$, $C_{\Delta g\varepsilon}$ are the covariance matrices between height-height, gravity height, gravity-gravity, slope-slope and slope-gravity. The covariance matrices D_{hh} and $D_{\varepsilon\varepsilon}$ contain the noise variance of the geoid height and slopes, respectively. The elements of the covariance matrices of (9.27) and (9.28) can e.g. be calculated according to a mathematical model fitted to the observations using a program like "covfit" in the GRAVSOFT library (Forsberg and Tscherning, 2008). If the different signal and error components are uncorrelated then the covariance values, C_{ij} and D_{ij}, are obtained by modifying the covariance to account for each of the signal and error components. For satellite observed sea surface height and the associated error the situation consists of several (assumed) uncorrelated terms and the covariances can be computed like

$$\begin{aligned} C_{hh} &= C_{NN} + C_{\xi\xi} \\ D_{hh} &= D_{e_{orbit}e_{orbit}} + D_{e_{tides}e_{tides}} + D_{e_{range}e_{range}} + D_{e_{rtrk}e_{rtrk}} + D_{e_{noise}e_{noise}} + D_{e_{env}e_{env}} \end{aligned} \qquad (9.31)$$

The covariance values can be obtained using the kernel functions. The kernel associated with the gravity field can be derived using the spherical harmonic approximation for T (3.14) and the *a-priori* variances. The covariance between the anomalous potential T in the points P(φ,λ) and Q(φ',λ') is expressed as

$$E(P,Q) = \sum_{i=2}^{\infty}\sum_{j=0}^{i} \sigma_i^{TT} P_i(\cos\psi) \qquad (9.32)$$

where σ_i^{TT} are degree variances and ψ is the spherical distance between the two points P and Q. Hence, eq.9.32 only depends on the distance between P and Q and neither on their locations nor on their azimuth (e.g. a homogeneous and isotropic kernel).

Expressions associated with geoid heights and gravity anomalies and DOV can be obtained by applying their respective functionals on E(P,Q), using covariance propagation like e.g. C_{NN}=L$_N$(L$_N$(E(P,Q))) for the geoid height following (5.48). Then

$$\begin{aligned} C_{NN} &= \sum_{i=2}^{\infty}\left(\frac{1}{\gamma}\right)^2 \sigma_i^{TT} P_i(\cos\psi) \\ C_{\Delta g\Delta g} &= \sum_{i=2}^{\infty}\left(\frac{i-1}{r}\right)^2 \sigma_i^{TT} P_i(\cos\psi) \\ C_{N\Delta g} &= \sum_{i=2}^{\infty}\left(\frac{i-1}{\gamma r}\right) \sigma_i^{TT} P_i(\cos\psi) \end{aligned} \qquad (9.33)$$

Accurate determination of the covariance function is important and is the subject of many studies in geodesy. An often used approach is to compute empirical covariances (program "empcov" of the GRAVSOFT package (Forsberg and Tscherning, 2008).

Subsequently, these values might be fitted to preselected model-covariance functions like the Tscherning/Rapp model.

Modelling of the covariance function associated with the gravity field is described in Knudsen (1987*a*). As degree variance model, a Tscherning/Rapp model described in (9.9) can be used. The modeled covariance function associated with height, gravity anomalies and DOV is shown in Figure 9.11 using degree variances for OSU91A to degree and order 360 (Rapp et al., 1991) with a scale factor of 0.207, gives the following typical covariance functions.

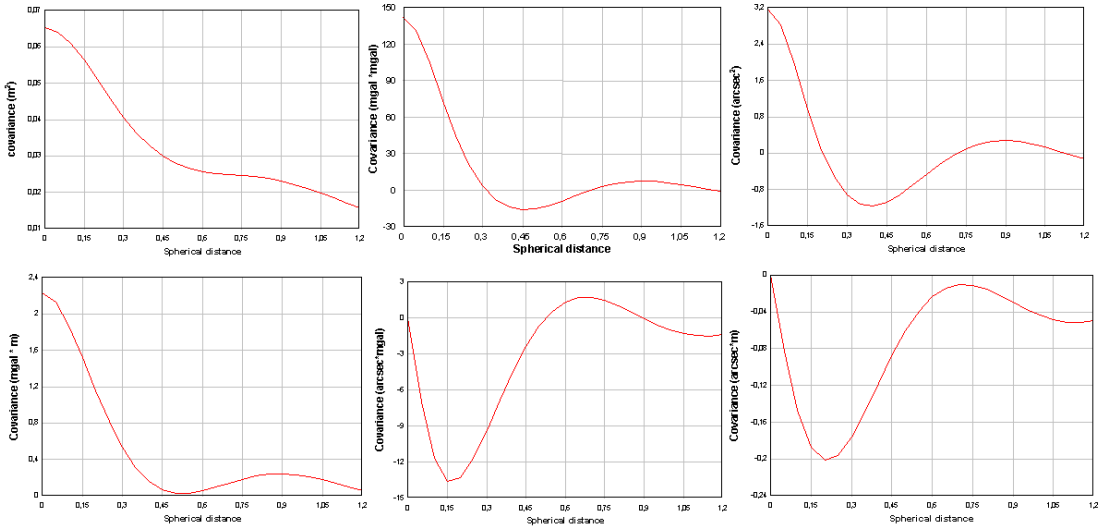

Figure 9.11 Covariance functions associated with height anomalies, gravity anomalies and DOV in the upper panels. Cross-covariance between gravity and height, DOV and gravity and DOV and height in the lower three panels (data from Tscherning 1997).

The ability to handle irregularly sampled data of various origins without the degradation due to interpolation makes LSC very well suited for computation of vertical gravity anomalies from along track satellite altimetry. The use of LSC should be considered upon creating local gravity fields where the computational cost is much smaller. A study by Hwang and Parson (1995) demonstrated the use of LSC for computing gravity field in a limited area around Iceland.

The ability of LSC to handle irregularly sampled data of different origin is shown in section 9.11, where the gravity field is predicted in coastal regions from altimetry and airborne gravity. In coastal regions LSC has the further advantage over methods the FFT method as the latter might suffer from high frequency noise due to the Gibbs phenomenon. (Bracewell 1978)

On global scales the computation of high-resolution gravity fields using LSC is simply not computationally feasible because of the huge amount of data ($>10^8$ altimetric observations globally). Even a computation of a local gravity field within a small cell of 1° by 1° can be problematic, as this cell might easily contains more than 2000 altimetric data points which needs to be analysed in order to compute accurate covariance functions. However, computational power is steadily increasing, and the use of LSC for future evaluation of global high resolution altimetric gravity field will become feasible in the near future. Therefore methods and approximations are currently being investigated in order to enable global computation of marine gravity using LSC.

9.7.1 Interpolation using least Squares Collocation

For the production of existing global altimetric gravity fields LSC can conveniently be used in combination with spectral methods like Fast Fourier Techniques (described in the next section). This section will show how LSC can efficiently used to perform the interpolation of the altimetric observations onto a regular grid which is required for the evaluation of gravity using fast spectral techniques.

Interpolation by LSC can be handled by the "geogrid" program in the GRAVSOFT software package (Forsberg and Tscherning, 2008) and will not be described here. This chapter will more focus on the adaption of the covariance function to local condition in the special case of interpolation of altimetric observations.

The local LSC prediction method in this program assumes a two dimensional isotropic covariance function described using a second order Markov function (Moritz 1987) as

$$C(r) = C_0(1+\frac{r}{\alpha})\, e^{(-r/\alpha)} \qquad (9.34)$$

r is the two-dimensional distance between the prediction point and computation point, and C_0 is the signal variance, and α is the correlation length (where a 50% correlation is obtained).

A special modification to the second order Markov function in (9.34) is sometimes applied for the interpolation of satellite altimetry due to the fact that the satellite observations are provided along individual tracks and an error might be associated with all observations along a specific track. This is particularly so in coastal regions where the spatial scale of the sea surface variability can become so short and large that the assumption used in the cross-over adjustment (modelled the signal using linear bias and tilt) becomes problematic.

A closer inspection of Figure 9.8 and Figure 9.18 illustrate this problem. To the north in the picture and in the German Bight in the lower right corner of the figure, some residual track related signal can be seen which also demonstrate that the crossover adjustment is not "perfect".

In order to limit the effect of this unwanted signal this error is modelled as an along track signal and in the interpolation this is accounted for by adding a covariance function for this error in the interpolation procedure. The error covariance function for this track related signal is applied to observations on the same track only (hereby assuming the error to be temporally uncorrelated)

Hence, for observations on the same track, the covariance function is modified to become

$$C(r) = C_0(1+\frac{r}{\alpha})\, e^{(-r/\alpha)} + D_0(1+\frac{r}{\beta})\, e^{(-r/\beta)} \qquad (9.35)$$

where D_0 is the variance of the residual sea surface height and the β is the correlation length of this signal. For observations on different tracks D_0 is fixed at zero yielding an expression similar to (9.34).

Interpolation will unavoidably filter the observations; so much case must be taken in creating the optimal interpolation to limit this effect to create the most accurate

gravity field anomalies. This along track modification to the second order Markov covariance function was originally derived for the KMS02 gravity field determination and subsequently refined for the DNSC08 gravity field prediction (Andersen and Knudsen 1997; Andersen et al. 2009). A practical use of this interpolation technique and the selection of interpolation parameters for the development of KMS02 will be shown in section 9.10.

9.8 Deterministic methods

Stokes integral formula and the solution to Stokes boundary value problem, have been described in chapter 3 and Stokes formula (3,100) have been widely used to compute geoid undulations from gravity anomaly observations primarily on land. On the ocean, the problem is reversed as the satellites observes residual geoid signal. With satellite altimetry, the inverse Stokes's formula, also known as the Molodensky's formula can be used to compute marine gravity anomalies from satellite altimeter derived sea surface heights (or geoid anomalies).

The inverse Stokes formula is a surface integral like

$$\Delta g_p = \gamma \frac{N_p}{r} - \frac{\gamma}{16\pi r} \iint_\sigma \frac{N - N_p}{\sin^3(\psi/2)} d\sigma \qquad (9.36)$$

where ψ is the spherical distance between the integration point (φ,λ) and the computation point (φ_p , λ_p).

Due to the properties of this integral kernel, the influence of more remote zones decreases rapidly and when using a remove/restore technique the integration radius can be limited to a few degrees (Wang 2001). There is a strong singularity at the innermost cell where $\sin^3(\psi/2)$ goes to zero. The approximation of this was treated by Lemoine et al. (1998).

The inverse Hotine's formula is related to the inverse Stokes formula and describes the relationship between the geoid undulations and the gravity disturbance and can be found in Zhang and Sideris (1996) and is similar to (3.20).

Gravity and geoid anomalies can also be derived from observations of north and east components of the DOV (ξ,η) using the inverse Vening Meinesz formula and the deflection-geoid formula (Hwang 1998).

$$\begin{Bmatrix} N \\ \Delta g \end{Bmatrix} = \frac{1}{4\pi} \begin{Bmatrix} R \\ \gamma \end{Bmatrix} \iint_\sigma (\xi \cos\alpha + \eta \sin\alpha) \begin{Bmatrix} C \\ H \end{Bmatrix} d\sigma \qquad (9.37)$$

where the kernel function H for the inverse Vening Meinesz formula related to deflection-geoid is given by

$$H(\psi) = \frac{\cos(\psi/2)}{2\sin(\psi/2)} \left(-\frac{1}{\sin(\psi/2)} + \frac{3 + 2\sin(\psi/2)}{1 + \sin(\psi/2)} \right) \qquad (9.38)$$

Where ψ is the spherical distance. The corresponding kernel function C for the deflection-geoid formula is given by

$$C(\psi) = -\cot\frac{\psi}{2} + \frac{3}{2}\sin\psi \qquad (9.39)$$

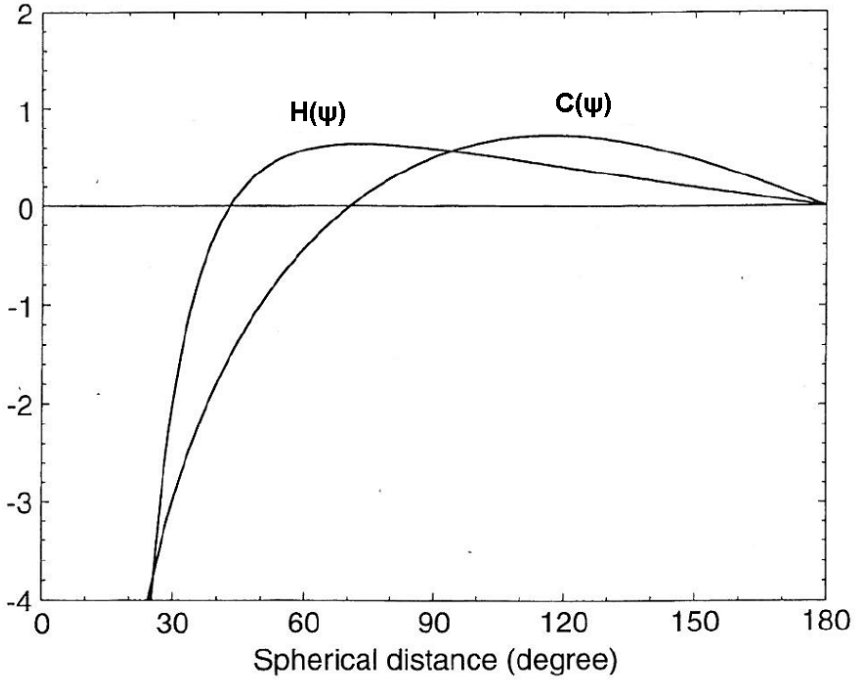

Figure 9.12 The functions H(ψ) and C(ψ) as a function of spherical distance ψ

Examples of the two kernel functions are shown in Figure 9.12. Formulas for handling the innermost zone effect around zero spherical distance can be found in Hwang (1998) who showed that the asymptotic behaviour of the *H(ψ)* and *C(ψ)* for small ψ reduces to

$$H(\psi) \approx -\frac{2}{\psi^2} \qquad C(\psi) = -\frac{2}{\psi} \qquad (9.40)$$

The global evaluation of both the inverse Stokes integral and the inverse Vening Meinisz integral are allied to the surface spherical harmonic analysis and synthesis processes, and all the above formulas requires globally distributed observations for the accurate computation of a single gravity value. However, some modifications are required to make high frequency global gravity field modelling using this approach feasible. This is the subject of the following section.

9.9 Fast spectral methods for altimetric gravity prediction.

Due to the enormous amount of altimetric data fast spectral methods have been used in all present global high-resolution gravity fields in one way or the other.

The most widely used spectral methods is the discrete Fast Fourier Techniques which has several advantages for fast computation, but which required data to be available as regular interpolated discrete values.

The fast spectral methods can be applied to evaluate the inverse Stokes integral (9.36) relating altimetric heights to gravity anomalies or for the the evaluation of the surface integrals related to DOV in (9.38) or for evaluating the fundamental equation of physical geodesy relating geoid height to gravity (9.23).

It is still assumed that the long wavelength of the gravity field is adequately provided by set of spherical harmonic constituents (EGM96 or EGM2008) and that the long wavelength part of the signal is completely removed using the remove-restore technique. This way, accurate but approximate evaluations can be made over a limited spherical cap centred at the evaluation point. This way only a limited part of the global dataset must be investigated for the computation. The advantage is that this opens up for parallel computing as different areas can be computed independent of each other on different computers.

The second assumption is the data are regularly distributed in a grid. Such approximation requires that another step is introduced, namely, an interpolation or a gridding. One possible interpolation process was described in section 9.7.1 using least squares collocation, but other interpolation processes like spline interpolation can also be used. Once data are available on a regular grid, the evaluation of the integral equations in (9.36) and (9.37) can very efficient be handled using spectral computational methods like Fast Fourier Transform.

9.9.1 Fast Fourier Techniques for altimetric gravity

One of the fundamental advantages in terms of high resolution marine gravity field prediction is that FFT directly gives the result on the same grid as the input grid. This means that a single FFT run immediately gives the result in all data points. Furthermore the increased computational power is more or less linearly dependent on the number of grid points which makes evaluation on very dense grids like global 1 or 2 minute grids possible. This means that the user should already in the interpolation step use the resolution of the wanted gravity grid.

The drawback of using FFT is the fact that data has to be provided on a homogenous interpolated grid which requires interpolation in the case of satellite altimetry. Furthermore FFT assumes data to be given at the same altitude but this is generally the case for satellite altimetry except for the few cases where data in e.g., lakes are used.

Gravity anomalies can be evaluated using spherical 1-D FFT methods. The spherical 1-D Fourier transformation was devised by Hagmanns et al (1993). In this method FFT is only applied in the longitude direction along each fixed parallel (φ_l). If a two dimensional grid is wanted, this can be achieved by combing sequences of 1-D FFT summarizing over all latitude bands. One dimensional spherical method has successfully been applied by e.g., Hwang et al. (1998) for recovering gravity anomalies from satellite altimetry.

2D FFT methods are available as spherical 2D FFT techniques (Strang van Hess, 1990) or multiband 2D spherical FFT technique (Forsberg and Sideris, 1993) as planar 2D FFT techniques (Schwarz et al., 1990). The detailed evaluation of the pros and cons of the various methods can be found in Part 7 of this book or in Liu and

Sideris (1997). The planar 2D requires the use of a flat Earth approximation and the introduction of a local Cartesian coordinate system.

For the sake of simplicity the derivation below is shown for a flat Earth approximation. Therefore, the computation of gravity anomalies is valid if the area only extends a few hundred kilometres in each direction (Part 7, section 7.2). The flat Earth approximation is applicable as the remove-restore technique using either EGM96 or EGM2008, typically removes wavelength longer than one hundred km ensuring that only data within a limited cap is needed for the computation.

In the flat Earth approximation a local Cartesian coordinate system (*x,y,z*) is introduced and the formulas 9.24 and 9.25 reduces to

$$\begin{aligned} \Delta g &= -\frac{\partial T}{\partial z} - 2\frac{T}{R_e} \approx -\frac{\partial T}{\partial z} \\ \xi_y &= -\frac{1}{\gamma}\frac{\partial T}{\partial y} \\ \eta_x &= -\frac{1}{\gamma}\frac{\partial T}{\partial x} \end{aligned} \qquad (9.41)$$

which in the frequency domain becomes

$$\begin{aligned} F(\Delta g) &\approx -|k|F(T) = -\frac{|k|}{\gamma}F(N) \\ F(\xi_y) &= -\frac{k_y}{\gamma}F(T) \\ F(\eta_x) &= -\frac{k_x}{\gamma}F(T) \end{aligned} \qquad (9.42)$$

Where *F(T)* represents the two dimensional discrete FFT of the grid of *T* values; $|k| = \sqrt{k_x^2 + k_y^2}$ and k_x, k_y are the wave-numbers equal to one over half the wavelength in the x and y direction, respectively.

Equation 9.42 shows, that the vertical derivative used to obtain gravity from residual geoid height in (9.41) is conveniently substituted by a Fourier transform and multiplication with the wave number followed by an inverse Fourier Transform.

The multiplication with the wave number amplifies short wavelength corresponding to high wave numbers, and filtering is required. This filtering process is treated in the section below.

Gravity anomalies can also be computed from DOV using the approximate relation (9.41) into the Laplace equation relating vertical gravity gradient with east and north DOV (Rummel and Haagmans, 1990).

$$\frac{\partial^2 T}{\partial^2 z} + \frac{\partial^2 T}{\partial^2 x} + \frac{\partial^2 T}{\partial^2 y} = 0 \Rightarrow \frac{\partial \Delta g}{\partial z} = -\gamma\left(\frac{\partial \eta}{\partial x} + \frac{\partial \xi}{\partial y}\right) \qquad (9.43)$$

In this way the vertical gravity gradient can be computed using a local grid of east and north DOV.

Applying the 2D Fourier transformation to (9.43) becomes

$$\frac{\partial(F(\Delta g))}{\partial z} = -i\gamma 2\pi (k_x F(\eta) + k_y F(\xi)) \qquad (9.44)$$

In Cartesian approximation Δg is harmonic too and so the formulas for upward continuation holds, which gives:

$$F(\Delta g(k,z)) = F(\Delta g(k,0)\exp^{(-2\pi|k|z)} \qquad (9.45)$$

Using (9.45) in (9.44) the relationship in the Fourier domain between the DOV and gravity anomalies is given in the form

$$F(\Delta g) = -i\frac{\gamma}{|k|}(k_x F(\eta) + k_y F(\xi)) \qquad (9.46)$$

So to compute gravity using altimetric DOV, initially grids of the north and east DOV components must be constructed (Sandwell and Smith, 1997; Hwang and Parson, 1996). Then these grids are Fourier transformed and then the grids are multiplied and added as given by 9.46 and the resultant grid is inverse Fourier transformed.

Using the planar approximation of the inverse Vening Meinesz formula (9.37) for the prediction of gravity using DOV and using the asymptotic representation in (9.40) for small spherical distances, Hwang (1998) demonstrated that the deterministic approach using the inverse Vening Meinesz formula also leads to (9.46), and that in the frequency domain it was equivalent to the stochastic approach of least squares collocation.

Finally a word on edge effects should be given. Before the FFT transform is applied to the residual geoid grid it is important to extend the computation region outside the data region and to apply a cosine taper to the outer parts of the grid. This is done to avoid spectral leakage caused by wavelengths that are not periodic within the area. Detailed description of this can be found in section 7.2.3

All available global altimetric gravity fields have take advantage of the FFT in their derivation in one way of the other for the computation of gravity on 1 or 2 minute global grids. The global marine gravity field by Sandwell and Smith (1997, 2009) and also the NCTU gravity field by Hwang (2002) applied the formulas 9.46 using DOV derived from sea surface slopes, whereas the KMS and DNSC fields (Andersen and Knudsen 1998; 2009) applied the upper formula in (9.42) to the gridded residual geoid signal derived from the altimetric sea surface heights.

9.9.2 Filtering

For satellite altimetry noise will always be present due to un-modelled tides, orbit errors or other contribution to residual sea surface height variability as described in section 9.5. This noise can be assumed to be of white noise nature, and will be amplified in the high-pass filtering operation of predicting gravity from geoid heights (9.42).

In order to limit this effect an optimal filter was designed that both handles the assumed white noise, but also handles the power spectral density of the gravity field signal. The power spectral density of the geoid spectrum is assumed to follow a Kaula rule power law (Kaula, 1966) who demonstrated, that the geoid height power spectrum decays like k^{-4} where k is the radial wavenumber.

The filtering is obtained by frequency domain least squares collocation with a Wiener filter (Nash and Jordan 1978, Forsberg 1997)

$$F(\Delta G) = \frac{\Phi_{N\Delta g}}{\Phi_{NN} + \Phi_{ee}} F(N) \qquad (9.47)$$

where Φ is the power spectral density and e is the assumed noise on the interpolated altimetric geoid undulations. Forsberg and Solheim (1988) confirmed that, assuming white noise signal and a Kaula rule for the spectral decay assumption, the Φ_{NN} will decay like k^{-4} and devised the following modification to eq. (9.42)

$$F(\Delta G) = \frac{k}{1 + ck^4} F(N) = k\,\beta(k)\,F(N) \qquad (9.48)$$

The parameter c is an empirical parameter which can be interpreted as a proxy of the "resolution" that can be obtained given data. The parameter is normally fine-tuned from the local variability of the gravity field and noise on the residual geoid heights (se Figure 9.16 below).
The "resolution" is here taken as the wavelength, corresponding to the wave-number k where $\beta(k) = 0.5$ corresponding to where $\lambda = 2\pi\, c^{1/4}$.

9.10 Practical computation of global high resolution marine gravity

For most practical purposes the global marine gravity fields are computed or evaluated on 1 or 2 minute global grids corresponding to 3.75 km or roughly 2 km at the Equator. Altimetry does not support 2 km spatial resolution with the densest cross-track and along track spacing between observations being around 6 km. Furthermore the interpolation and the filtering applied in (9.48) suppresses wavelength shorter than roughly 10 - 15 km. The one minute grid is generally chosen to limit the loss of information in the interpolation process. For the DNSC08 gravity field, the 1 minute resolution is also chosen to ease the joint use of the suite of global DNSC08 fields (gravity, bathymetry, mean sea surface, mean dynamic topography, and prediction error) by giving all on a common global grid.

Below, the way that the KMS02 and DNSC08 global marine gravity fields were computed are presented to illustrate the various parameters choice in order for the reader to be able to understand the physical meaning of the choices as well as to assist the reader to derive their own altimetric gravity fields making their own experiments and choices.

The way the gravity field is practically computed is by patching up the Earth in a number of tiles or regions and to compute each tile or region separately. The 2º latitude by 10º longitude used for KMS02 can be seen in Figure 9.15 below. For the derivation of the DNSC08 gravity field smaller tiles of the size of 2º latitude by 5º longitude were used. For both fields a 0.5º additional margin outside the data region was added to taper the geoid signal to zero at the boundaries in order to avoid Gibbs effects in the FFT computation.

The interpolation of scattered along-track anomalies onto a regular grid is the first step in the process. This step is crucial to the accuracy of the gravity field so much

care must be taken in choosing the optimum parameters for the covariance function (9.35) used in this step. For the KMS02 gravity field, the following parameter choices were made for the signal variance (C_o) and the correlation length (α).

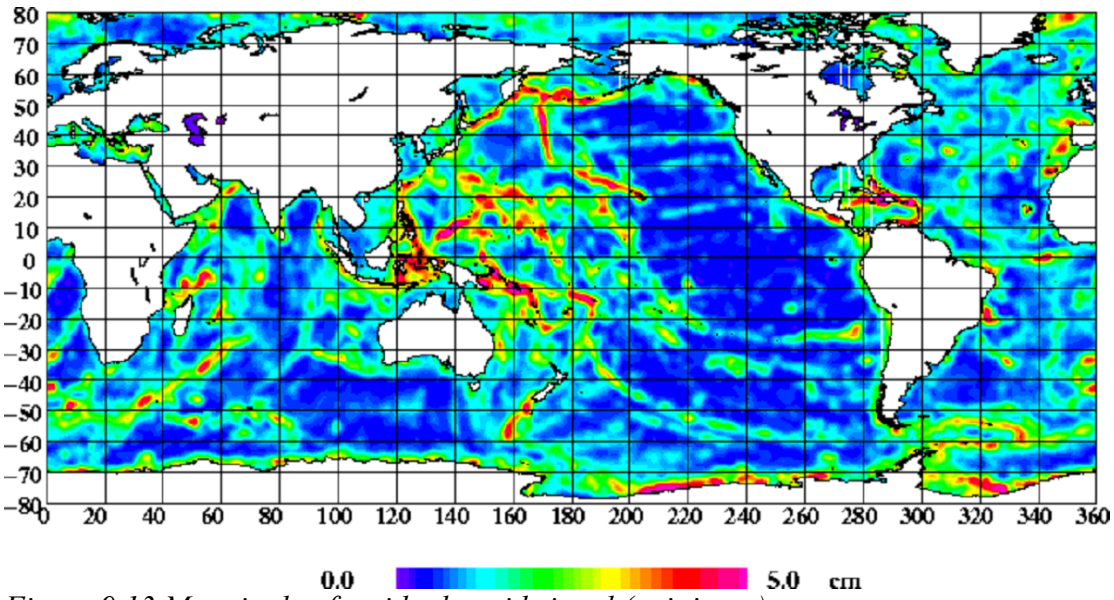

Figure 9.13 Magnitude of residual geoid signal (unit is cm).

Figure 9.13 shows the magnitude of the residual geoid signal which was used for the computation of the signal variance (C_o). The signal and hence it variance, is seen to be largest in the tectonic active regions like the spreading and subduction zones.

The next parameter in (9.35) is the correlation length of the residual geoid signal (α). The correlation length is shown in Figure 9.14 from a computation in 1° by 1° blocks. The correlation length largely reflects the depth of the ocean with relative small correlation length found for regions of smaller depths which are especially found along the spreading zones.

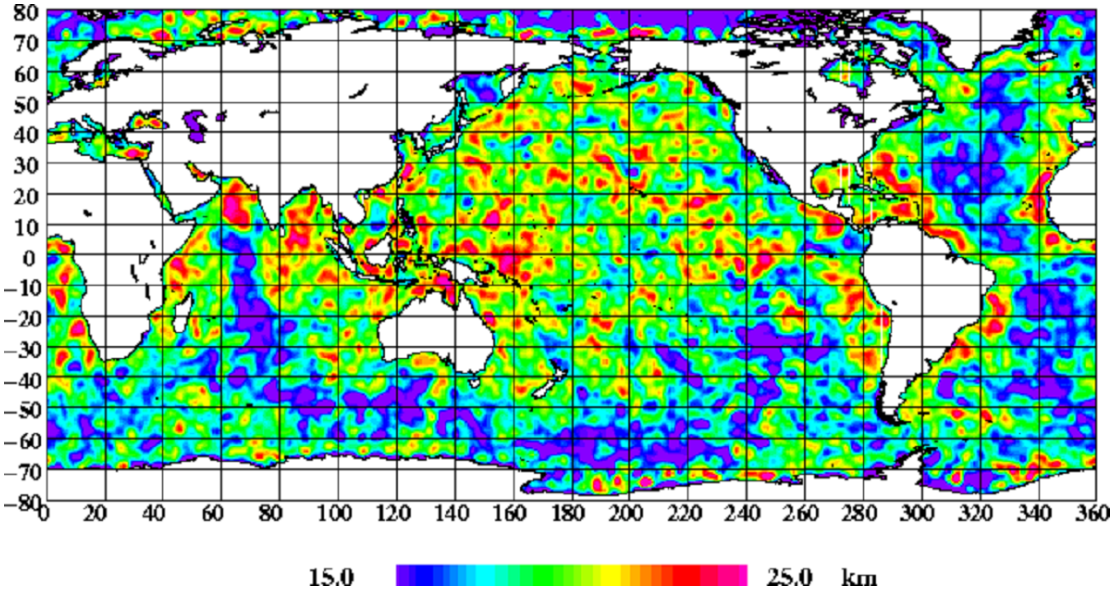

Figure 9.14 Correlation length of the signal (α) computed as the half-width of the empirical covariance functions in 1° by 1° blocks.

The additional two parameter introduced into the second order Markov covariance function to model residual along-track errors are the variance (D_o) and correlation length (β) of this signal. The correlation length (β) was empirically determined to be 100 km assuming the error to be of long wavelength compared with the correlation length of the residual gravity signal (α).
In order to avoid problems with possible correlation between the quantities in (9.35), the D_o was kept fixed for the interpolation in each 2º by 10 º tile. The value should reflect regions of high oceanographic noise. Hence it was approximated by a scaled version of the RMS of the sea surface height computed from six years of ERS-2 repeat observations and the magnitude range between $(0.5 \text{ cm})^2$ and $(4 \text{ cm})^2$. The average RMS of the sea surface variance within each tile is shown in Figure 9.15.

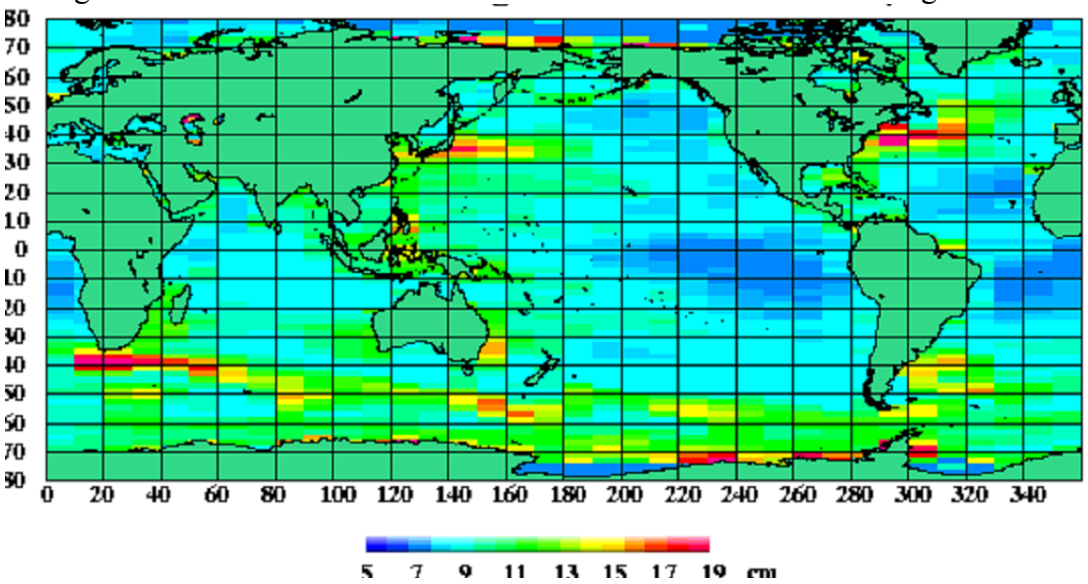

Figure 9.15 The RMS of residual sea surface height used to determine the along track residual sea surface variance D_o parameter in (9.35) averaged over each 2° latitude by 10 ° longitude tiles. This clearly indicates the location of major current systems.

The interpolated residual geoid height grids in each tile were then used to compute gravity anomalies using the multiband spherical 2D FFT technique. The conversion of geoid heights to gravity anomalies enhances shorter wavelength, and the Wiener filter described in 9.48 was applied using the filter parameter shown in Figure 9.16.

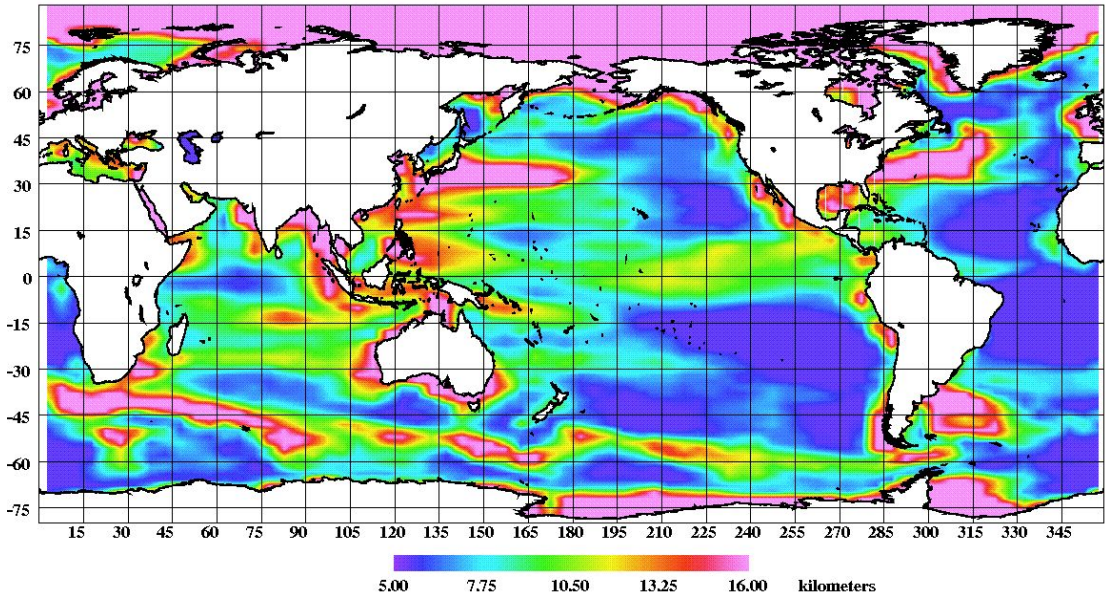

Figure 9.16 The resolution parameter c in (9.47) used for the filtering of the gravity field (DNSC08GRA).

Like several parameters for the interpolation, this parameter is strongly linked with the standard deviation of the sea surface height (se figure 9.5). The resolution parameters reflect the sea surface variability with high values in the major global current systems like the Gulf Stream, the Kuroshio and the Antarctic Circumpolar Currents. It should be interpreted in the way that increased filtering, thus resulting in "lower resolution" (higher *c*) is required in the most energetic regions to account for the increased "noise". Furthermore the presence of sea ice at latitude north and south of 70° requires increased filtering in these regions.

The DNSC08 and KMS02 were both derived in a global set of tiles (Andersen and Knudsen 1998; 2009) but with different tile sizes and different processing parameters. For KMS02 the mosaic of 90 times 72 tiles were subsequently patched together, but for DNSC08 the smaller were tiled together with tapered overlay to avoid gradients along the tile-edges that could occasionally be seen in KMS02.

Finally the long wavelength gravity effect was restored using EGM96 in the case of KMS02 and EGM08 in the case of DNSC08 to give the total gravity field signal. This process also adds gravity on land. The final DNSC08 Global marine gravity field is shown in Figure 9.17

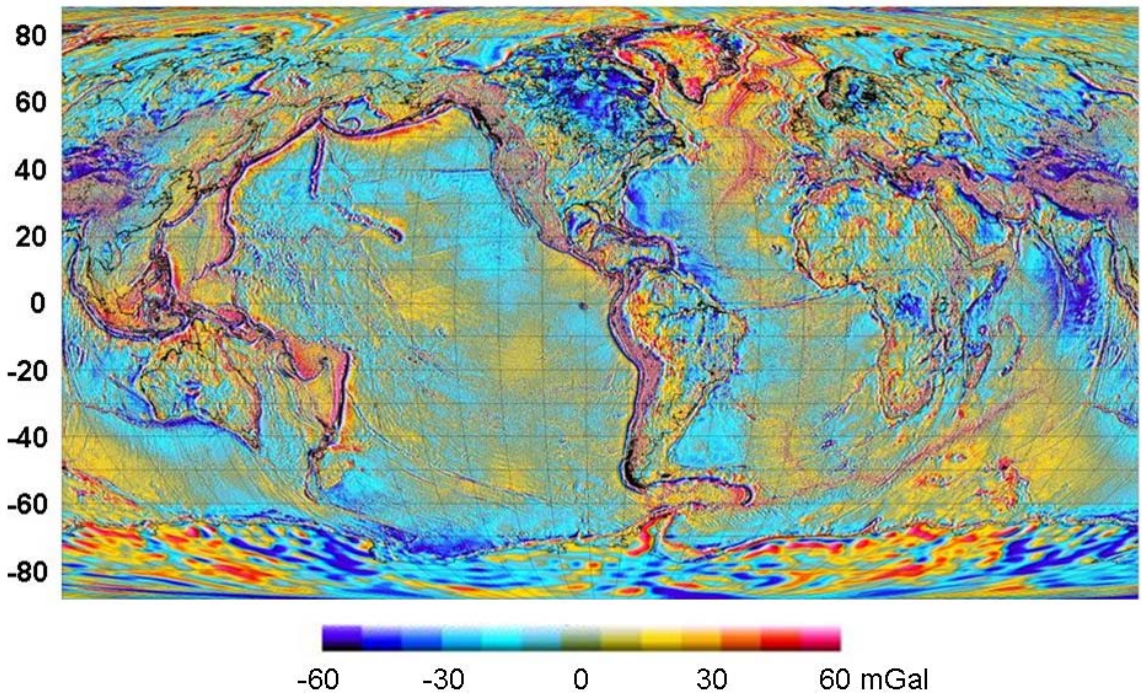

Figure 9.17. The DNSC08 global gravity field. The altimetric gravity field over the oceans has been augmented with interpolated values from EGM2008 over land.

In this section the basic choice of parameter and their physical interpretation and fine-tuning was described for the conversion between gridded altimetric observations for the derivation of global marine gravity field. The subsequent section shows an example of the computation in one extended 5 by 9 degree tile in the North Sea with a geological interpretation.

9.10.1 North Sea example.

This section illustrate the practical steps in computing marine gravity from satellite altimetry starting using the same dataset as presented in Figure 9.1 and 9.8. Here the process starts with residual geoid heights after the EGM96 have been removed and the data have been crossover adjusted.

The sea surface height observations representing the residual geoid height are shown in Figure 9.18. Only ERS-1 GM data are considered in this example and only one 5° latitude by 9° longitude tile in the North Sea is considered. The standard deviation of the altimetric residual geoid heights are 4.8 cm with maximum value of 59 cm.

Some residual track-related errors are still visible after the crossover adjustment by the two blue arrows in Figure 9.18 to the north towards the southern tip of Norway and to the south eastern part of the North Sea in the German Bight. Notice that the errors to the north are associated with tracks that also appear in the German Bight. These small errors can be handled using the extension to the Gauss Markov covariance function (9.34) as shown in (9.35).

In Figure 9.18 the thick red arrow indicate a small positive signal which will be shown below to be associated with a strong gravity signal related to a buried volcano.

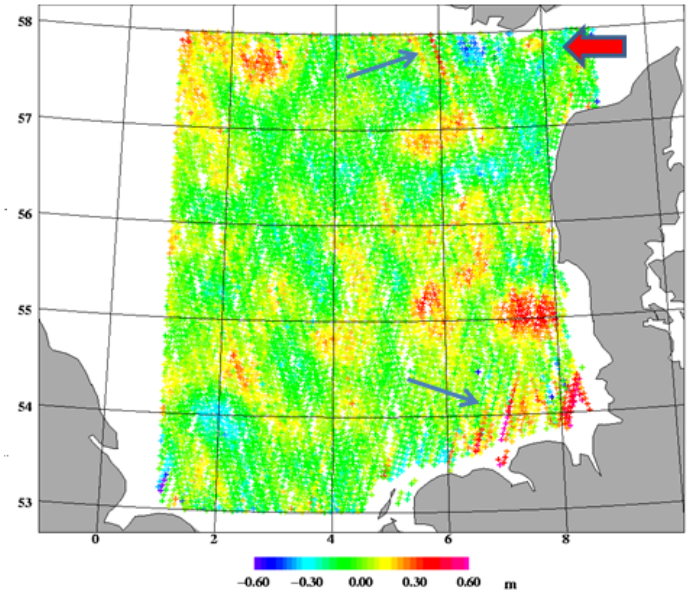

Figure 9.18. The crossover adjusted ERS-1 geodetic mission sea surface height observations in the North Sea relative to the EGM96 geoid. The blue arrows indicate regions of imperfect crossover adjustment and the red arrow the location of a buried volcano.

These values are subsequently interpolated by LSC using the modified second order Gauss Markov covariance functions formulas (9.35) with the fine-tuned parameters for signals and correlations length shown in Figure 9.14 and Figure 9.15. The result of the interpolated residual geoid height grid on 1 minute resolution is shown in Figure 9.19. The standard deviation of the interpolated grid is 4.1 cm with maximum value of 42 cm.

Notice that the residual along track geoid signal in the northern part of the region has been removed in the interpolated field. Also notice how the interpolation un-avoidable extrapolate signal towards and onto the coast.

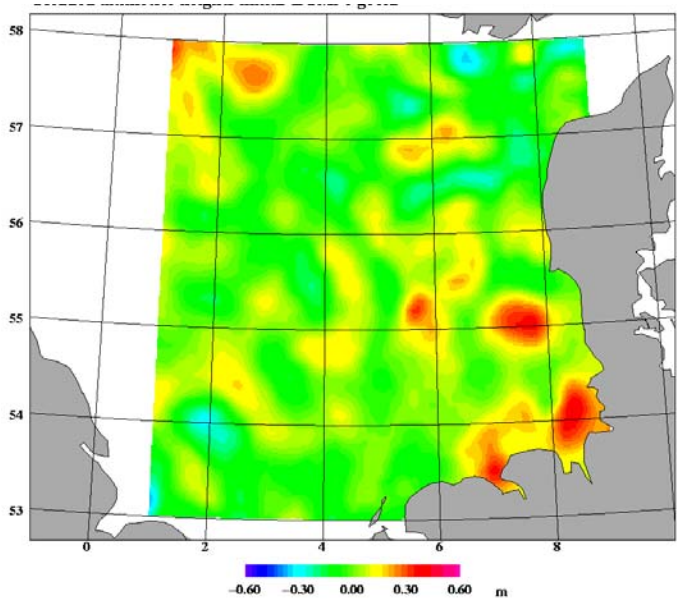

Figure 9.19. The interpolated residual sea surface height observations.

Subsequently the interpolated residual geoid height values in Figure 9.19 were used to compute residual gravity anomalies using FFT applying a Wiener filter (9.48) with a choice of "resolution parameter" of 15 km taken from an inspection of Figure 9.16. The residual gravity signal relative to EGM96 had a standard deviation of 5.2 mGal with a maximum value of 38 mGal on top of the buried volcano close to the southern tip of Norway marked in Figure 9.18.

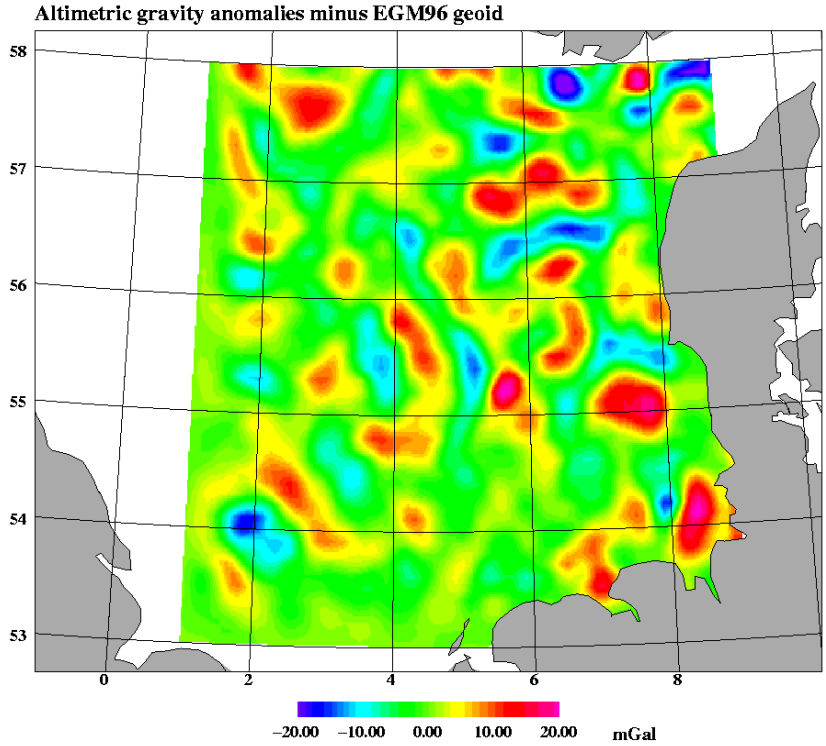

Figure 9.20. The residual gridded gravity anomalies (relatively to EGM96).

The final step in the gravity field prediction is to restore the EGM96 gravity contribution gives the full marine altimetric gravity field which is shown in Figure 9.21. Now the standard deviation has been increased to 15 mGal and the maximum value is 42 mGal and the minimum value is -41 mGal. Comparison with local marine gravity observations in the region reduces from more than 8 mGal to better than 4 mGal.

The most distinct feature is a buried volcano south of Norway which is not resolved by EGM96, but clearly resolved using satellite altimetry. This peak anomaly of 42 mGal is found right at this buried volcano and the peak negative value of -41 mGal is found just to the east of this.

This free-air gravity field map also shows other distinct geological features related to the tectonics of the North Sea. One is the north-south going "Horn Graben" close to Denmark which is not resolved from EGM96. The other is the "Viking Graben" which is not very well resolved by EGM96 either.

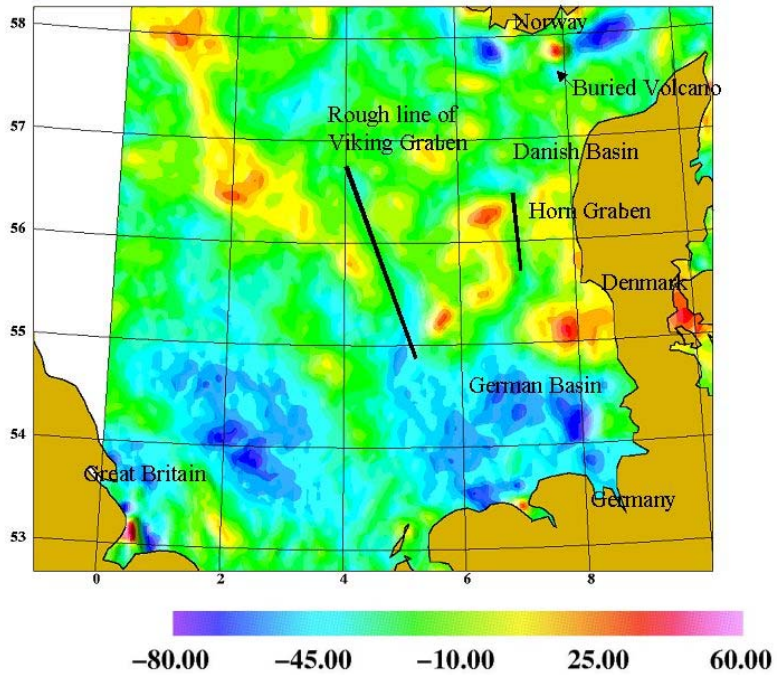

Figure 9.21. The altimetric marine gravity field with EGM96 restored. All values are in mGal. Some major geological features of the region have been added to the map.

9.11 Accuracy of present-day altimetric marine gravity fields.

Since the late 1990th several global marine gravity fields have become available on 1 or 2' resolution for free download on the Internet: The NCTU fields (Hwang et al. 2002); the Sandwell & Smith fields – versions from 9.1 to version 18.1 (Sandwell and Smith 1997); the KMS02/DNSC08 fields (Andersen and Knudsen 2005), and the GSFC fields (Wang 2001). During the last decade waveform retracking in one form or the other has been applied by Laxon and McAdoo (1998) who retracked altimetry in the Arctic Ocean using a robust retracker, Hwang (2003) who retracked altimetry in the China Sea; Fairhead et al. (2004) who retracked/repicked data in several coastal regions, and finally the DNSC08 and SS who applied retracking to the later versions of their marine gravity field (Andersen et al., 2009; Sandwell and Smith 2005; 2009).

Numerous local and global marine gravity anomalies have been created using a variety of successful techniques (e.g., Haxby (1987); Balmino et al. (1987); Sandwell (1992); Knudsen (1991); Knudsen et al. (1992); Tscherning et al. (1993); CLS (Hernandez and Shaeffer 2000), NCTU (2001) and OSU (Yi 1995).

In order to illustrate the history of improvement in altimetric marine gravity field mapping over the last 10-15 years 321.400 unclassified marine gravity observations with accuracy of 2-4 mGal were provided by the National Geospatial-intelligence Agency (NGA) for the validation of altimetric gravity fields. This dataset covers the region between 25ºN and 45ºN and 275ºE and 325ºE corresponding to the region from the US east coast and out to the Mid-Atlantic spreading zone. The Gulf Stream flows northeast across the region and introduces an error of the order of 2-3 mGal because of increased sea surface height variability. Therefore, the comparison should NOT be viewed as representative for the general accuracy of global altimetric gravity fields, but more as an illustration of the general improvement in gravity field modeling during the last decade. Actually, the Gulf Stream region is one of the regions where

altimetry performs the worst compared with marine gravity observations and where most smoothing has to be applied as shown in Figure 9.16.

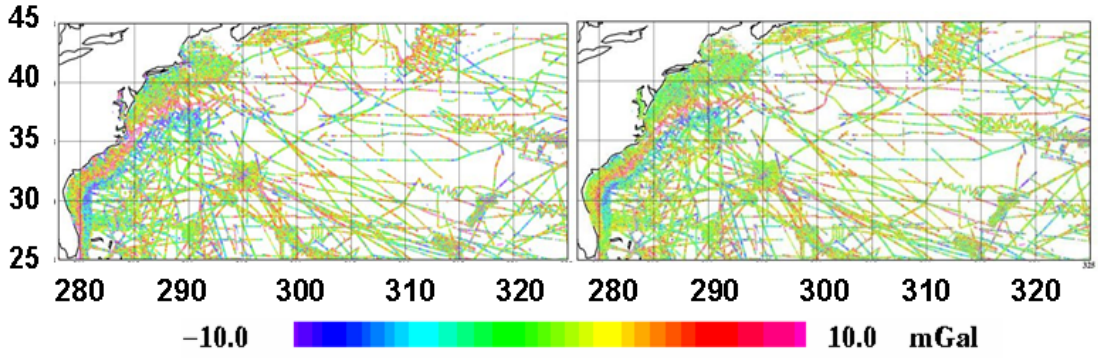

Figure 9.22 Color coded difference between interpolated satellite altimetry gravity and 321.400 marine data in the Northwest Atlantic Ocean. The difference between marine data and the KMS02 global marine gravity field is shown in the left panel, and the corresponding comparison for DNSC08 is shown in the right panel. A closer inspection reveals that the DNSC08 is significant better in coastal regions.

321.400 obs	Standard Deviation (mGal)	Maximum Difference (mGal)
KMS99	5.69	73.74
KMS02	5.05	49.38
DNSC08	3.92	36.91
EGM2008	3.94	36.90
SS V12.1	5.79	82.20
SS V16.1	4.88	45.29
SS V18.1	3.98	36.99
GSFC 00.1	6.14	89.91
NCTU01	6.10	92.10

Table 9.2. Comparison with 321.400 marine gravity field observations in the Gulf Stream region. For each of the global marine grids the standard deviation and the maximum difference are given. SS fields by Sandwell & Smith (1997; 2009); KMS02/DNSC08 by Andersen and Knudsen (1998; 2009); EGM2008 by Pavlis et al. 2008); GSFC field by Wang (2001) and NCTU01 is by Hwang et al. (2002);

A detailed comparison with this dataset is presented in Table 9.2 and the point by point difference between measured and interpolated gravity field values in the region is shown in Figure 9.22. A total of 9 global gravity fields released during the last decade have been tested. The oldest fields are the KMS99 field (1999), followed by the GSCF 0.1 (2000), the NCTU 01 (2001) and SS V12.1 (2001) and KMS02 (2002). All of these have standard deviation with the 321400 gravity observations higher than 5 mGal.

A stready improvement in the accuracy of altimetric marine gravity field has been observed during the last decade. With the release of EGM2008 and the global gravity field (DNSC08 and SS V18.1) a consistent comparison below the 4 mGal level has been achieved. In terms of improvement this corresponds to more than 20%

improvement in standard deviation compared with global marine gravity fields 7-10 years ago. One should notice that part of the 321.400 marine gravity field observations have entered into the EGM2008 geopotential model as 5 minute mean anomalies.

The detailed comparison in Figure 9.22 between individual marine gravity observations and interpolated gravity from KMS02 (left panel) and the DNSC08GRA (right panel) initially looks identical. However a close inspection of particularly the coastal regions indicates that DNSC08 is substantially better than KMS02 which is the effect of retracking and improved ocean tide modelling. Both maps show a red/blue anomaly pattern which closely follows the Gulf Stream. This could indicate that the correction for mean dynamic topography (ζ_{MDT}) using the PGM2007A mean dynamic topography model complete to degree and order 50 (Andersen and Knudsen 2009; Pavlis et al. 2007) and used for the derivation of EGM2008 does not have adequate resolution, and that future corrections for mean dynamic topography should remove even higher degree and order of the signal.

9.12 Integrating marine, airborne and satellite derived gravity

Marine gravity field are available from various different sources, like gravimeters onboard marine vessels (e.g., ships and submarines), onboard aircrafts, manually operated in the field, and finally from satellite altimetric measurements. These different data sources should not be considered as competitors of gravity information but rather a great opportunity to have complimentary sources of gravity information and the only way to create a truly global gravity field including the Polar Regions.

Airborne gravimetry is a fast and economic method for local to regional scale gravity mapping. Some of the biggest advantages are the uniform and seamless coverage of land and sea, and the ability to cover remote and otherwise inaccessible areas. The bias free property of airborne gravity data obtained by spring type gravimeters is also an important point for geodetic applications; see Childers et al. (2001) and Olesen et al. (2000*)*. Ship borne gravity measurements are still one of the the most accurate sources of gravity at sea, but the cost is large and furthermore the ship needs a minimum water depth in order to be feasible.

Airborne and marine gravimeters observe the gravity directly, and can be used to determine (any) offset, which might be present in the altimetric gravity field. The three set of data are shown in Figure 9.23 for the test area on the west coast of Greenland around the Disko Bay.

The gravity field derived from altimetric residual geoid height observations h can be merged with airborne and/or marine gravity observations $\Delta g'$ using Least Squares Collocation. The expression for gravity and a-posteriori variance $\sigma^2_{\Delta g}$ on the predicted gravity anomalies Δg are

$$\Delta g = \left(C_{\Delta g h} C_{\Delta g \Delta g}\right) \begin{pmatrix} C_{hh} + D_h & C_{h\Delta g'} \\ C_{\Delta g' h} & C_{\Delta g' \Delta g'} + D_{\Delta g'} \end{pmatrix}^{-1} \begin{pmatrix} h \\ \Delta g' \end{pmatrix} \qquad (9.49)$$

and

$$\sigma^2_{\Delta g} = C_{\Delta g \Delta g} - \left(C_{\Delta g h} C_{\Delta g \Delta g}\right) \begin{pmatrix} C_{hh} + D_h & C_{h\Delta g'} \\ C_{\Delta g' h} & C_{\Delta g' \Delta g'} + D_{\Delta g'} \end{pmatrix}^{-1} \begin{pmatrix} C^T_{\Delta g h} \\ C^T_{\Delta g \Delta g} \end{pmatrix} \qquad (9.50)$$

C_{hh} , $C_{\Delta gh}$, $C_{\Delta g\Delta g}$ are the covariance matrices between height-height, gravity-height, gravity-gravity. The covariance matrices D_h and $D_{\Delta g'}$ contain the noise variance of the geoid height and gravity observations, respectively. Gravity anomalies with hyphen like Δg´ are the observed gravity from altimetry and/or ship. Δg are predicted gravity anomalies.

9.12.1 East Greenland airborne and altimetric gravity example

The Disko Bay (Illulisat fjord) coastal region located on Greenland's west coast around latitude of 69°N and longitude 55°W is used as test region, as it has good coverage of altimetric, marine and airborne observations as seen in Figure 9.23. This area has seasonal ice cover and ice drift. A covariance function based on airborne gravity residuals has been estimated and an analytic expression has been determined (*Knudsen 1987a*).

For airborne gravity, an error model which takes into account the correlated noise is used in this study. However, the effect of incorporating this feature was found to be insignificant. This implies that even though the airborne data are filtered along track, they may be considered as point values for our use. Predicted gravity anomalies, as well as their associated error estimates, are finally derived from the normal equation solution. More information about the study can be found in Olesen et al. (2001).

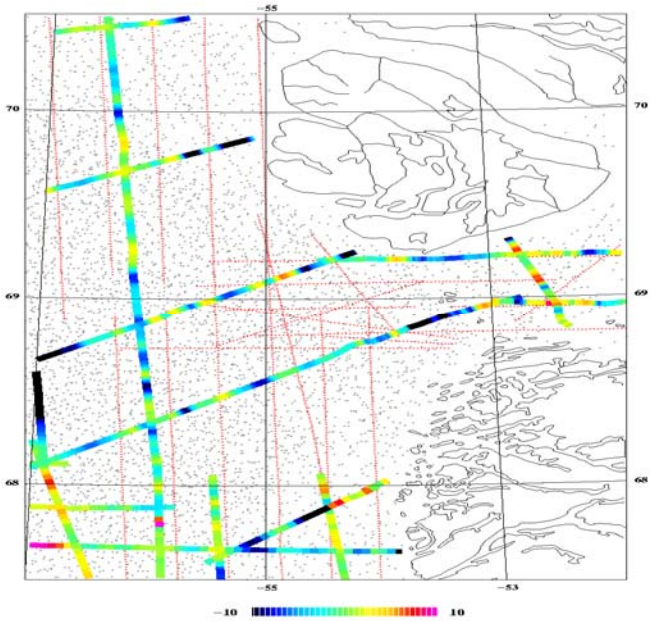

Figure 9.23. Test area on the west coast of Greenland: The distribution of satellite altimetry (gray dots) and airborne gravity (aligned black dots) together with the difference between marine gravity and collocation results based on sea surface heights observations and airborne gravity.

Input data	Mean	Std. dev.	Abs. max.
Airborne gravity	-0.5	6.9	26
Satellite altimetry	-9.5	5.4	24
Satellite altimetry + airborne gravity	-0.7	3.6	18

Table 9.3 Comparisons with marine gravity data (in mGal). Both the altimetric and airborne gravity field has been interpolated onto the location of the marine observations. Direct comparisons between co-located airborne observations and marine observations compares better than 2 mGal (Olesen et al. 2000)

The result in Table 9.3 shows a very big improvement with the marine observations with the agreement being improved from 6.9 to 3.6 mGal. Similarly the bias of –9.5 mGal between marine and altimetric gravity is reduced to –0.7 by the combined use of altimetry and airborne gravity. This demonstrates the potential for improving coastal marine gravity field by merging different types of observations.

9.13 Altimetric gravity research frontiers

The previous sections have shown that the global altimetric gravity fields are generally very accurate in the open ocean, but in coastal and Polar Regions the error increases and this is naturally a focus area for future research. Gravity recovery is particularly difficult in these regions, but on here the largest improvement can still be gained from a dedicated effort in improving the accuracy of the sea surface height observations.

The problems in shallow water and Polar Regions are due to several factors: The waveform shape of the returned radar pulse will only infrequently follow a Brown model and hence data are frequently rejected by the automatic retracking by the space agencies. The presence of a coast will also distort the part of the illuminated region by the altimeter or the radiometer used to determine the range or range corrections. Sea state is also changing close to the coast and particularly the spatial extent of the tidal signal is scaled down creating very complex tidal patterns which furthermore include resonance and overtones. For the coastal regions, the use of spectral methods like the Fourier Transform will also be problematic even though the removal of the highly accurate EGM2008 model ensures that the recovered signal is not so much distorted by the presence of land.

For the next generation of global altimetric gravity fields dedicated effort into research in the following areas will be needed it for further gravity field improvement:

- Inclusion of new data types (ICESat, Cryosat-2, Sentinel-3)
- Improving the altimeter range corrections
- Improving the ocean tide correction
- Altimeter waveform re-tracking.

In the following an introduction into the problems and importance of these effects on gravity field determination will be presented with examples from ongoing research. Large part of the investigation relates directly to improving the accuracy of the sea surface height observations and hence lowering the error e on the altimetric observations (Eq 9.19)

9.13.1 ICESat and Cryosat-2

ICESat laser altimetry is a relative new and complementary data source to conventional radar altimetry (*Zwally et al.* 2002). The important aspect of ICESat is the fact that it has an inclination of 86° which brings it 400 km closer to the Pole

than the ERS and Envisat satellites. In principle laser data can be processed and used very much like radar altimetry. For the DNSC08GRA these data were used in the partly ice-covered parts of the Arctic Ocean (between 70°N - 86°N, 100°E - 270°E) and at latitudes above 80°N in all of the Arctic Ocean in order to extend the MSS and gravity field towards the North Pole. Only a few months of the ICESat data were available for DNSC08 and since the termination of the mission in 2010 a total of around 19 month was recorded. One further advantage of ICESAT is its much smaller footprint compared with radar altimetry which means that it can in principle resolve shorter wavelength of the gravity spectrum. The footprint of the laser has a radius of roughly 70 meters observing at each 120 meters along track where as the radius of conventional radar altimeter (ERS and Jason type) has a radius of 5-10 km depending on the sea state.

Cryosat-2 was successfully launched in 2010. To meet the challenges of measuring ice-sheet changes, Cryosat-2 carry a sophisticated radar altimeter called SIRAL (Synthetic Aperture Radar Interferometric Radar Altimeter). It is capable of carrying out Delay-Doppler observations in one direction during flight which means that the resolution compared with conventional altimetry is increased by a factor of 20 to around 300 meters. However over most of the oceans Cryosat-2 will operate as a conventional altimeter. The accuracy of Cryosat-2 will be well below the 1-cm level (Rainey et al., 2005) making it significantly better than conventional satellite altimeters as seen in Table 9.1. This means that besides being useful for the determination of the thickness of the ice, the Cryosat-2 can be used to recover gravity anomalies over the ocean with unprecedented accuracy compared with conventional satellite altimetry.

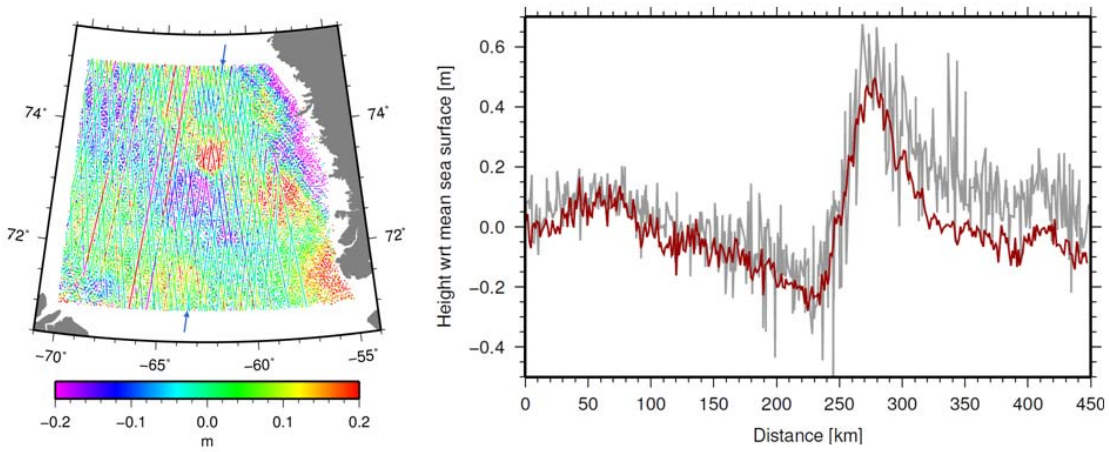

Figure 9.25. Residual sea surface height observations in the Baffin Bay from ERS-1 and the first 3 month of SAR processed Cryosat-2 data. The profile marked with an arrow in the left figure is shown in the right figure with distance from the northern point.

The first 3 month of Cryosat-2 SAR retracked residual sea surface height data in the Baffin Bay is shown in Figure 9.25 overlayed the residual sea surface height from ERS-1 used for the prediction of DNSC08. Similar to the processing of ERS-1 (se section 9.3-9.5) wavelength longer than 200 km have been removed from Cryosat-2 but no crossover adjustment were preformed.

One SAR 5 Hz profile is marked in the left Figure with a blue arrow. The figure to the right shows the Cryosat-2 residual sea surface height (relative to the DTU10

Mean sea surface and not to the geoid) in red and ERS-1 observations (grey) within 5 km across-track from the SAR profile. Dramatic improvement in accuracy of the Cryosat-2 data is clearly visible compared with the older ERS-1 satellite data.

Cryoat-2 will furthermore improve the mapping of the Arctic Ocean as it has an inclination of 92 degrees bringing it 200 km from the North Pole and for coastal regions the footprint of some 300 meters of the Delay-Doppler signal will enable gravity field mapping much closer to the coast.

9.13.2 Altimeter range corrections.

The determination of sea surface height close to the coast degrades due to the fact that several range corrections degrade as the altimeter approaches the coast. The radiometer used to correct the altimeter for both, dry and wet troposphere, ionosphere has a much larger footprint than the altimeter and particularly the wet troposphere correction is affected. Although much smaller than the dry tropospheric range correction in magnitude, the wet troposphere correction is far more complex showing rapid variations in both time and space and therefore also needs careful attention in the coastal region. The correction can vary from just a few millimeters in dry, cold air to more than 30 cm in hot, wet air.

The footprint of the radiometer is dependent on the height of the spacecraft and the scanning frequency of the radiometer, but typical values of the footprint of the main beam ranges between 20 and 30 km. This is considerably larger than the 4-10 km footprint of the altimeter as illustrated in Figure 9.25 for a pass across the Western Mediterranean Sea. Consequently, the radiometer is contaminated by the presence of land much earlier than the altimeter, as the spacecraft approaches and coast and generally the main beam is affected up to 30 km from the coast. The wet troposphere correction derived from the on-board radiometer is similarly affected, and currently intensive research is performed to improve the wet troposphere correction in coastal regions (e.g., Eymard and Obligis, 2006)

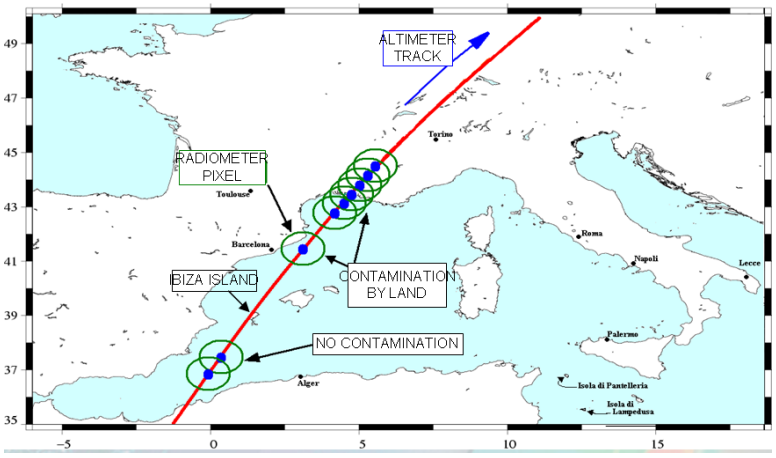

Figure 9.25. An example of a Jason-1 track crossing the western Mediterranean Sea. Blue dots indicate the footprint of the altimeter and the green circles shows the size of the main radiometer beam. Figure from Eymard amd Obligis (2006).

The analysis by Andersen and Scharroo (2009) showed that the accuracy of the wet troposphere correction degrades from around 1.1 cm in the open ocean to roughly half the accuracy around 30 km from the coast.

9.13.3 Ocean tides

The largest contributor to sea surface height error in shallow water is unquestionably due to errors in present day ocean tide models (Andersen and Scharroo, 2009). Even, though the determination of the ocean tides have dramatically improved since the launch of TOPEX/Poseidon and most recent investigations indicate that global models are now accurate to around 1-2 cm in the global ocean (Andersen et al., 2006; Shum et al., 1997), there are still problems close to the coast due to the fact that the tidal signal is scaled down and becoming increasingly complex with the presence of overtides in shallow water regions (Andersen, 1998; Andersen et al., 2006)

Figure 9.26 shows the difference in gravity field mapping for the Gulf of Maine using two different ocean tide models. The plot to the left is a comparison between marine gravity and interpolated gravity using KMS99 which used FES94 in its derivation. The figure to the right represents the differences between marine gravity and interpolated gravity from KMS02, which used the GOT00.2 ocean tide model (Ray 2001). The largest improvement are clearly seen north of 42°N, which is the location of the shelf break, which indicate the significant improvements from the use of GOT 00.2 ocean tide model. Since this investigation was performed, ocean tide modelling has improved even further with the release of new ocean tide models called GOT 4.7.

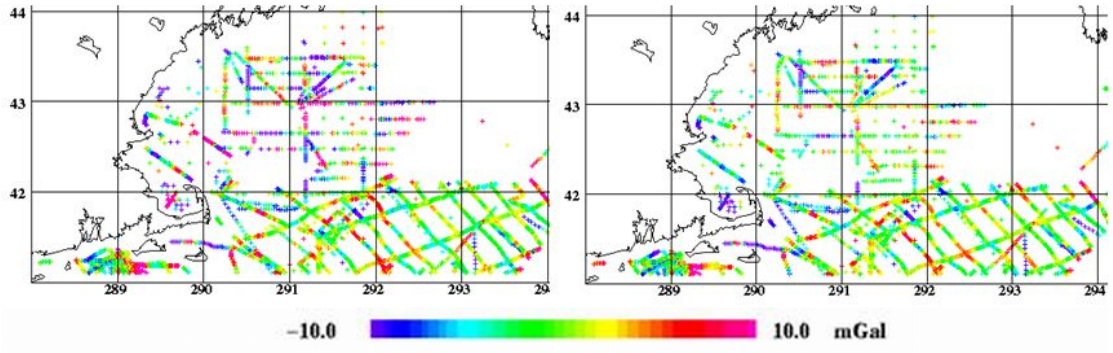

Figure 9.26. The difference between marine observations and altimetric gravity in parts of the Gulf of Maine are colored. Left shows the differences for KMS99 and right the differences for KMS02. The color scale ranges +/- 10 mGal, and the major difference between the two fields is explained by the use of GOT 00.2 compared with FES94 for the KMS99 gravity field to the left.

In the deep ocean, recent investigations showed that ocean tide has a height accuracy of around 1.4 cm (Bosch 2008). However, global ocean tide models still have errors exceeding 10-20 cm close to the coast as also demonstrated by Ray (2008). Such signal can easily generate 5 - 10 mGal gravity error very close to the coast. So improved coastal ocean tide modeling is still one of the key to improved altimetric gravity field recovery in shallow water regions in the future.

9.13.4 Retracking in coastal and Polar Regions

As the satellite approaches the coast the characteristics of the sea surface changes, and it is important to retrack the existing GM data using more tolerant methods in order to increase the amount of data available to derive altimetric gravity. Similarly, it is important to retrack satellites to increase the accuracy of the sea surface height observations. This process involves two runs of retracking – a so called double retracking - where the first retracking run is performed to increase the number of observations, whereas the second run is performed to increase the accuracy of the sea surface height retrieval also demonstrated in Figure 9.10.

The Geosat GM does not benefit much from retracking as it was very carefully investigated and retracked originally by the US Navy. The data was recently recompiled from various archives, reprocessed and retracked at NOAA, who kindly provided the dataset to the scientific community (Lillibridge et al., 2005).

Due to special properties and the high inclination of the ERS-1 GM mission, the data from this satellite clearly gains most from retracking. With the Arctic Ocean being mostly permanently ice-covered, and the ERS-1 satellite covering up to the 82 parallel, retracking is the only way of obtaining altimetric gravity data at high latitudes where very few of these data resemble open ocean Brown waveforms.

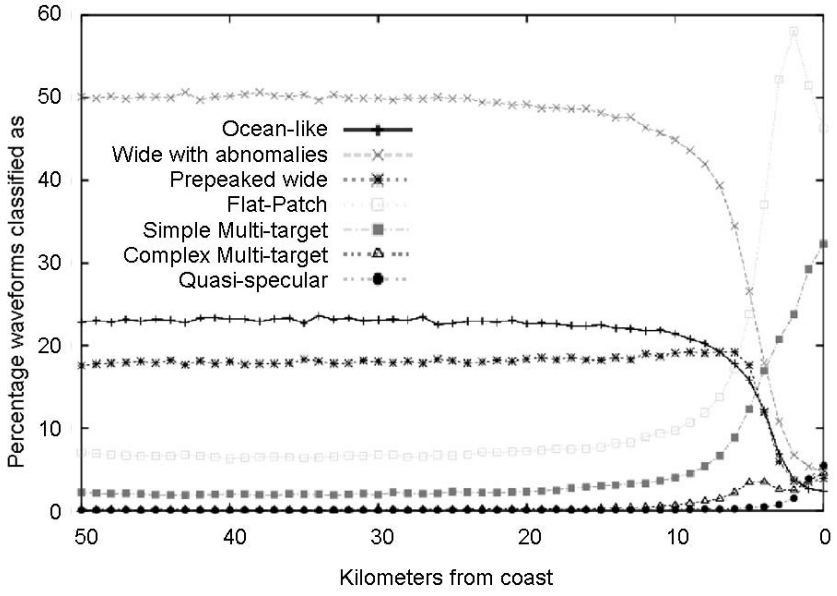

Figure 9.27. Waveform shape distribution from 18 Hz un-averaged observations in global coastal zone (excluding sea-ice) from the ERS1 GM as a function of the distance to the coast. Detailed description of waveform characteristics can be found in Dowson et al. (2006).

Another benefit of tolerant retracking of the ERS-1 data is the fact that the waveform changes rapidly in complexity as the altimeter approached the coast. Numerous different echo shapes appear in the coastal zones caused by a variety of surface effects including land contamination of the echo, off-ranging to inland water, and the presence of unusually calm water in sheltered areas. For a detailed description of different waveforms se Dowson et al. (2006).

Even though coastal zone echoes are complex and rapidly changing, the waveforms can be successfully retracked. Figure 9.27 illustrate that within 10 km of the coast, a rapid increase in non-Brown model waveforms is seen; within 5 km of the coast the majority of the echoes are non Brown model shaped. For the derivation of the DNSC08 gravity field, the Earth and Planetary Science Lab (EAPRS) expert system (Berry et al. 1997; Berry et al. 2005) was adapted to retrack 10 complex waveform shapes of the ERS-1 GM waveforms corresponding to ice, inland water and land. In order to include ocean waveform retracking the Southampton Ocean Center ocean retracker (Challenor and Srokosz 1989) was added to the system.

Due to the presence of sea-ice in Polar Regions, these will be the regions where retracking using multiple tolerant retrackers will provide the most new data and the most significant improvements to gravity field determination. The region east of Greenland (75ºN < latitude < 80 ºN, 320ºE < longitude <350 ºE) is well known for the presence of sea ice. Here the number of ERS-1 data points that can be retrieved from retracking is increased from 750 data points (un-retracked) to 22200 data points (retracked) using the more tolerant retrackers as seen in Figure 9.28. Even data in the narrow fjords are recovered.

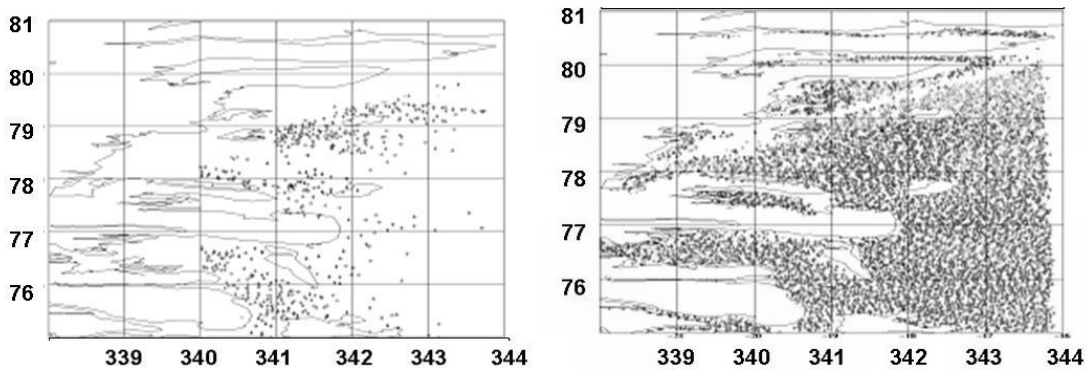

Figure 9.28. *Altimetric height observations in the ice-covered regions east of Greenland. The upper figure shows the number of data points that can be retrieved using standard ESA retracked 1Hz data. The lower figure shows the amount of 1 Hz data that can be retrieved using more tolerant retrackers.*

This vast improvement in data carries forward into an improvement of the derived gravity field. This can be seen from a comparison with 900 airborne gravity data from the Greenland/Svalbard KMS9803 survey bounded by 77ºN-80ºN, 30ºW-5ºE. The accuracy of these airborne measurements is better than 2 mGal (Olesen, 2003)

Table 9.4*. Comparison with 900 airborne gravity observations from the KMS9803 airborne survey. The standard deviation and maximum difference between the airborne observation and various gravity fields are given.*

900 points	Std (mGal)	Max (mGal)
KMS02	9.4	51.2
Laxon and McAdoo (97)	7.2	46.2
ArcGP (01-06)	5.8	34.4
SS 16.1 / 18.1	8.2 / 5.9	44.9 / 37.4

DSNC08	4.1	24.0

The results of the comparison with 900 airborne gravity observations are shown in Table 9.4 for six different gravity fields; the KMS02, Laxon and McAdoo (version 97), ArcGP (version (01-06), SS v. 16.1 and v. 18.1 and DNSC08GRA. The Laxon and McAdoo polar gravity field (version 97) was developed using an early attempt with tolerant retracking of the ERS data (Laxon and McAdoo, 1998). The ArcGP gravity field is derived from a combination of data from different sources such as marine, airborne, altimetry etc. (Kenyon and Forsberg, 2008). For KMS02 the lack of retracked altimetry over the ice means that this field is not good at all. The Laxon and McAdoo gravity field from retracked ERS data is significantly better, and the ArcGP compilation of data performs even better. The DNSC08GRA is partly based on the ArcGP data, as ArcGP is part of data dataset used to derive the EGM2008 geoid and gravity field. The huge amount of new data that can be retrieved using suite of tolerant retrackers and particularly the sea-ice designed retracker (Berry et al., 2005) brings the standard deviation of the comparison for DNSC08GRA all the way down to 4.1 mGal. In terms of variance reduction this is nearly a 6-times improvement over KMS02.

Appendix 9.1. Data resources

Altimetry Data.

Some of the major distributors of satellite altimetry are the following:

Radar Altimetry Database system (RADS)
http://rads.tudelft.nl

Archiving Validation, interpretation of satellite data (AVISO)
www.aviso.oceanobs.com/en/altimetry/index.html

National Ocean and Atmosphere Administration (NOAA)
http://ibis.grdl.noaa.gov/SAT/ocean_links.html

Jet Propulsion Lab (JPL-PODAAC)
http://podaac.jpl.nasa.gov/DATA_CATALOG/index.html

International Altimeter Service (IAS):
http://ias.dgfi.badw.de/IAS

Altimetric gravity field ressources.

DTU Space (DNSC, DTU gravity field models)
http://space.dtu.dk (data and models)

University of California, San Diego (Sandwell and Smith gravity field models)
http://topex.ucsd.edu/marine_grav/mar_grav.html

NCTU National Chaotung University (Taiwan)
The NCTU1 global marine gravity field model is available on request from Cheinway Hwang at hwang@geodesy.cv.**nctu**.edu.tw

Arctic Gravity Field Project (ArcGP)
Arctic gravity field grid
http://earth-info.nga.mil/GandG/wgs84/agp/readme_new.html